Geothermal Membrane Distillation for Large-Scale Use

Desalination and Water Purification Research and Development Program Report No. 240

REPORT DOCUMENTATION PAGE

Form Approved
OMB No. 0704-0188

The public reporting burden for this collection of information is estimated to average 1 hour per response, including the time for reviewing instructions, searching existing data sources, gathering and maintaining the data needed, and completing and reviewing the collection of information. Send comments regarding this burden estimate or any other aspect of this collection of information, including suggestions for reducing the burden, to Department of Defense, Washington Headquarters Services, Directorate for Information Operations and Reports (0704-0188), 1215 Jefferson Davis Highway, Suite 1204, Arlington, VA 22202-4302. Respondents should be aware that notwithstanding any other provision of law, no person shall be subject to any penalty for failing to comply with a collection of information if it does not display a currently valid OMB control number.
PLEASE DO NOT RETURN YOUR FORM TO THE ABOVE ADDRESS.

1. REPORT DATE *(DD-MM-YYYY)* 03-09-2021	2. REPORT TYPE Final	3. DATES COVERED *(From - To)* 1/1/2019 – 09/30/2021	
4. TITLE AND SUBTITLE Geothermal Membrane Distillation for Large-Scale Use		**5a. CONTRACT NUMBER** Agreement No. R18AC00107	
		5b. GRANT NUMBER	
		5c. PROGRAM ELEMENT NUMBER	
6. AUTHOR(S) Frank Huang, Professor		**5d. PROJECT NUMBER**	
		5e. TASK NUMBER	
		5f. WORK UNIT NUMBER	
7. PERFORMING ORGANIZATION NAME(S) AND ADDRESS(ES) New Mexico Institute of Mining and Technology 801 Leroy Place Socorro, NM 87801		**8. PERFORMING ORGANIZATION REPORT NUMBER**	
9. SPONSORING/MONITORING AGENCY NAME(S) AND ADDRESS(ES) Bureau of Reclamation U.S. Department of the Interior Denver Federal Center PO Box 25007, Denver, CO 80225-0007		**10. SPONSOR/MONITOR'S ACRONYM(S)** Reclamation	
		11. SPONSOR/MONITOR'S REPORT NUMBER(S) DWPR Report No. 240	

12. DISTRIBUTION/AVAILABILITY STATEMENT
Available from the National Technical Information Service,
Operations Division, 5285 Port Royal Road, Springfield VA 22161

13. SUPPLEMENTARY NOTES
Available online at https://www.usbr.gov/research/dwpr/DWPR_Reports.html

14. ABSTRACT
For the western states where untapped brackish groundwater and geothermal resources are abundant, geothermal membrane distillation (GMD) offers a unique opportunity to desalinate geothermal brackish groundwater with the innate heat to supplement freshwater demand. A pilot-scale direct contact membrane distillation (DCMD) system was deployed to the second largest geothermally-heated commercial greenhouse in the U.S. for field testing. A techno-economic model calibrated with the field data was developed to evaluate the cost-effectiveness of large-scale GMD plants. The findings of this project show that large-scale GMD systems have very low commercial viability with currently available equipment.

15. SUBJECT TERMS
Direct contact membrane distillation, geothermal, greenhouse, pilot-scale, PTFE, hollow fiber membrane, techno-economic model

16. SECURITY CLASSIFICATION OF:			17. LIMITATION OF ABSTRACT	18. NUMBER OF PAGES	19a. NAME OF RESPONSIBLE PERSON Alyssa Aligata
a. REPORT U	b. ABSTRACT U	THIS PAGE U			19b. TELEPHONE NUMBER *(Include area code)* (303) 445-2264

Standard Form 298 (Rev. 8/98)
Prescribed by ANSI Std. Z39.18

Geothermal Membrane Distillation for Large-Scale Use

Prepared for the Bureau of Reclamation Under Agreement No. R18AC00107

by

Frank Huang, New Mexico Institute of Mining and Technology

Mission Statements

The U.S. Department of the Interior protects and manages the Nation's natural resources and cultural heritage; provides scientific and other information about those resources; and honors its trust responsibilities or special commitments to American Indians, Alaska Natives, and affiliated Island Communities.

The mission of the Bureau of Reclamation is to manage, develop, and protect water and related resources in an environmentally and economically sound manner in the interest of the American public.

Disclaimer

The views, analysis, recommendations, and conclusions in this report are those of the authors and do not represent official or unofficial policies or opinions of the United States Government, and the United States takes no position with regard to any findings, conclusions, or recommendations made. As such, mention of trade names or commercial products does not constitute their endorsement by the United States Government.

Acknowledgments

Acronyms and Abbreviations

Acronym or Abbreviation	Definition
AGMD	air gap membrane distillation
CPVC	chlorinated polyvinylchloride
DCMD	direct contact membrane distillation
FPGA	field programmable gate array
GMD	geothermal membrane distillation
HE	heat exchanger
HFM	hollow fiber membrane
LEP	liquid entry pressure
LMH	liters per meter squared, per hour
MAE	mean absolute error
MED	multi-effect distillation
MD	membrane distillation
MSF	multi-stage flash
NIPS	nonsolvent-induced phase separation
NTU	number of transfer units
PP	polypropylene
PTFE	polytetrafluoroethylene
PVDF	polyvinylidene fluoride
Reclamation	Bureau of Reclamation
RO	reverse osmosis
SEM	scanning electron microscopy
SWMD	sweeping gas membrane distillation
TDS	total dissolved solids
TIPS	thermally-induced phase separation
TPC	temperature polarization coefficient
TP	temperature polarization
USGS	United States Geological Survey
VAMD	vacuum assist membrane distillation
VPG	vapor pressure gradient
XRD	X-ray diffraction

Measurements

Acronym or Abbreviation	Definition
bar	pressure
cm	centimeter
°C	degree Celsius
°F	degree Fahrenheit
gpm	gallon per minute
hp	horsepower
kΩ	kilo-ohm
L/m^2-hr	liter per meter squared-hour
MPa/cm	mega-pascal per centimeter
m^2	meter squared
m/s	meter per second
μg/L	microgram per liter
μm	micrometer
mN/m	millinewton per meter
mg/L	milligram per liter
nm	nanometer
psi	pound per square inch
wt%	weight percent
W/m-K	watts per meter-Kelvin

Variables

Symbol or Abbreviation	Definition
a_w	water activity
B	pore geometry coefficient
B_m	mass transfer coefficient
c_f	salt concentration of the feed
$C_{p,f}$	specific heat capacity of water at constant pressure on the feed side
$C_{p,p}$	specific heat capacity of water at constant pressure on the permeate side

Symbol or Abbreviation	Definition
D_w^k	Knudsen diffusion coefficient
D_{w-a}^0	pressure-independent molecular diffusion coefficient
$d_{h,f}$	hydraulic diameter for the feed
$d_{h,p}$	hydraulic diameter for the permeate
h_f	feed heat transfer coefficient
h_p	permeate heat transfer coefficient
K	entrance/exit head loss coefficient for the pilot DCMD module
k_g	thermal conductivity of the gas trapped in the pores
k_m	thermal conductivity of the membrane
k_{pol}	thermal conductivity of the membrane polymer
k_f	thermal conductivity of the feed
k_p	thermal conductivity of the permeate
L	length of the module
MW	molecular weight of water
N	flux
n_f	total number of fibers in the module
n_{max}	maximum number of fibers that can fit within a certain diameter module
P_f	feed hydraulic pressure
P_p	permeate hydraulic pressure
p_s	saturated water vapor pressure of the saline solution
p_v	saturated water vapor pressure of pure water
$p_{v,mf}$	vapor pressure of the feed at the membrane surface
$p_{v,mp}$	vapor pressure of the permeate at the membrane surface
R	universal gas constant or inner radius of the tube
T_f	bulk feed temperature
T_{fm}	membrane surface temperature of the feed
T_p	bulk permeate temperature
T_{pm}	membrane surface temperature of the permeate
$T_{f,1}$	feed inlet temperature
$T_{p,1}$	permeate inlet temperature
$T_{f,2}$	feed outlet temperature
$T_{p,2}$	permeate outlet temperature
V_f	feed flow rate
V_p	permeate flow rate

Symbol or Abbreviation	Definition
v_0	velocity through the tube
v_w	fluid velocity normal to the tube wall of the membrane
v_s	shell velocity
v_l	lumen velocity
γ	surface tension of water
$\gamma_{l,\,new}$	corrected water surface tension
γ_l	surface tension for pure water at standard temperature and pressure
θ	contact angle of the membrane
r_{max}	maximum pore size of the membrane
ρ_m	membrane density
ρ_{pol}	polymer density
ϵ	membrane porosity
χ_{NaCl}	mole fraction of NaCl in the feed solution
χ_w	liquid mole fraction of water
ΔHLV	latent heat of vaporization of water
δ	thickness of the membrane
μ_b	bulk fluid viscosity of either the feed or permeate
μ_m	viscosity observed at the feed or permeate membrane surface
$\mu_{m,f}$	viscosity of the feed at the membrane surface
$\mu_{m,p}$	viscosity of the permeate at the membrane surface
μ	bulk fluid viscosity
Nu	Nusselt number
Gz	Graetz number
Re	Reynolds number
Pr	Prandtl number

Table of Contents

List of Figures

List of Tables

Appendix A – Images of the Completed Pilot-Scale DCMD System

This page intentionally left blank.

Executive Summary

The goal of this project was to perform pilot-scale field testing of geothermal membrane distillation (GMD) so that a techno-economic model could be developed to assess the commercial viability of full-scale GMD systems. For the western states where untapped brackish groundwater and geothermal resources are abundant, GMD offers a unique opportunity to desalinate geothermal brackish groundwater with the innate heat to supplement freshwater demand. A pilot-scale direct contact membrane distillation (DCMD) system was constructed and deployed to Masson Farms in New Mexico. Masson Farms is the second largest geothermally-heated commercial greenhouse in the U.S. Geothermal brackish groundwater of 80-90 °C is utilized for space heating at the facility. The cooled geothermal fluid downstream of the heat exchangers was used as the source water of the DCMD pilot system so that the residual innate heat (about 70°C) could be utilized to produce distilled water for irrigation prior to re-injection into the formation. Field data were collected at Masson Farms and used to tune a DCMD performance model developed based on energy/mass conservation and heat/mass transfer. The calibrated performance model was then integrated into a techno-economic model for cost assessment of large-scale DCMD plants.

The developed techno-economic model was used to evaluate the capital cost of a DCMD plant with conditions similar to those of Masson Farms (water production of 160 gallons per minute, feed inlet temperature of 80°C, and permeate inlet temperature of 45°C). With full-scale (14- by 40-inch) DCMD modules, it would cost about $150 million to build the plant with the specified capacity. About 55 percent of the capital cost was for the air-cooled heat exchangers that were used to remove the thermal energy deposited on the permeate stream via DCMD. Due to the inefficiency of low-grade heat transfer, a tremendous number of heat exchangers was required in order to maintain the distillation efficiency of the DCMD modules. If the flow-distribution design of the DCMD modules were improved to increase water flux, the capital cost of the DCMD plant could be reduced by two-thirds to about $54 million, with the heat exchangers still bearing over 50 percent of the total cost. Based on the findings of this project, large-scale GMD systems have very low commercial viability with currently available equipment.

This page intentionally left blank.

1. Introduction

Traditionally, the bulk of the U.S. water demand has been satisfied by a combination of surface water and fresh groundwater. However, as climate and land use change, resources deplete, and population grows, these sources are not expected to suffice; thus, unconventional water resources are needed to prevent dire socio-economic consequences. Brackish groundwater represents a substantial but largely untapped resource (Tidwell et al. 2014). A conservative low estimate for the volume of extractible brackish groundwater is about 3 billion acre-feet, more than 35 times the amount of fresh groundwater used in the U.S. during 2010 (Stanton et al. 2017). The utilization of this unconventional water resource, however, is very limited. Data from the U.S. Geological Survey (USGS) indicates that an estimated 10,000 acre-feet/day of brackish groundwater was used in the U.S. in 2010, which constituted only 4 percent of the total groundwater use (Stanton et al. 2017). In the Western U.S., substantial amounts of fresh water are used for agriculture activities. For example, in California, Arizona, and most western states where pressures on water availability are especially intense, up to 80 percent of total water use is consumed by irrigated agriculture (Gleick 2010). The strain on the water supply is further exacerbated by projected climate change, which may result in 10-20 percent reduction of groundwater recharge across southwestern aquifers by the year 2100 (Stanton et al. 2017). Therefore, it is especially urgent in this region to explore technologies that can utilize the vast quantity of the unconventional resource of brackish groundwater as a supplement to or replacement for freshwater supply.

1.1. Project Background

1.1.1. Problem and Needs

Reverse osmosis (RO) is a well-established technology for brackish water desalination. However, it is relatively energy-intensive, at times requires a higher level of pretreatment to reduce membrane fouling, and has limited options for in-land concentrate management. For the western states where untapped brackish groundwater and geothermal resources are abundant, membrane distillation (MD) offers a unique opportunity to desalinate geothermal brackish groundwater with innate heat to supplement freshwater demand. In contrast to RO, MD is not a pressure-driven process and relies mainly on the vapor pressure gradient across hydrophobic membranes to drive the production of distilled water. Membrane distillation is especially attractive to horticulture and aquaculture operations that utilize geothermal brackish water as the heating source and where the demand of quality water for irrigation or cultivation is high. For these operations, MD provides distinct advantages of:

1. Reduced energy and freshwater footprints with utilization of the existing geothermal brackish fluid as the co-located source of water and energy;
2. Reduced membrane fouling potential due to the non-pressure-driven nature; and
3. Existing geothermal formation as the potential repository for the desalination concentrate, given the better chemical compatibility.

1.1.2. Objectives

The goal of the project was to evaluate commercial viability of geothermal membrane distillation (GMD), specifically direct contact membrane distillation (DCMD), for desalinating brackish groundwater. Specific objectives of the project were to:

- Perform pilot-scale testing to develop performance models for system scale-up, evaluate long-term field performance, and collect design and operational data for full-scale systems; and
- Develop a techno-economic model to evaluate the cost-effectiveness of full-scale GMD systems.

1.2. Overview of the MD Technology

The MD process consists of three steps: evaporation of water from the feed side, migration of water vapor through membrane pores, and condensation of water vapor on the permeate side of the hydrophobic membrane (Susanto 2011). There are four basic MD configurations: DCMD, air gap membrane distillation (AGMD), sweeping gas membrane distillation (SWMD), and vacuum assist membrane distillation (VAMD; Simone et al. 2010; Wang and Chung 2015). The simplest configuration is DCMD in which the condensed permeate is in direct contact with the membrane and the temperature difference across the membrane induces the vapor pressure difference. Heat loss by conduction, however, is highest in this configuration. In AGMD, a thin air gap is introduced between the membrane and a condensation surface. The downside of this configuration is that the vapor transport through the air layer is one magnitude less than that of the membrane. SWMD and VAMD are generally used for separation processes in chemical and food industries and may not be cost effective for water treatment (El-Bourawi et al. 2006).

MD membranes are typically made from dope solutions that consist of hydrophobic polymers and organic solvents. Hydrophobicity is an important characteristic of MD membranes; hydrophobicity aids in the prevention of pore wetting and can be measured by water contact angles. In order to overcome pore wetting, it has been suggested that increasing membrane hydrophobicity is more effective than decreasing the membrane pore diameter (Lawson and Lloyd 1997). The three most prevalent polymers used for MD are polyvinylidene fluoride (PVDF), polypropylene (PP), and polytetrafluoroethylene (PTFE). Their properties and fabrication methods are shown in Table 1 (Wang and Chung 2015; Lawson and Lloyd 1997; Tomaszewska 1996).

Table 1. Properties of PVDF, PP, and PTFE

Polymer	Surface energy (mN/m)	Contact angle with water	Thermal conductivity (W/m-K)	Melting temperature (°C)	Fabrication methods
PVDF	30.3	91°	0.19	170	NIPS*, TIPS** Electro-spinning
PP	30	102°	0.17	176	Melt-extrusion, TIPS
PTFE	9-20	109°	0.25	327	Melt-extrusion

* nonsolvent-induced phase separation
** thermally induced phase separation

Performance of DCMD is measured primarily based on the level of water flux observed for the process. Water flux is the volumetric flow rate of permeate passing through unit area of membrane and is commonly expressed as liters of permeate per meter squared of effective membrane area, per hour (L/m²-hr, or LMH). Water flux of a DCMD module can be affected by operating conditions, membrane characteristics, and module configurations as described in the following sections.

1.2.1. Vapor Pressure Gradient

The overall performance of a DCMD module is dependent on the transmembrane vapor pressure gradient (VPG). The magnitude of the gradient is determined by the difference between the feed and permeate saturated water vapor pressures that can be estimated using the Antoine equation as shown in Equation 1. The water activity of the saline solution and the saturated water vapor pressure of pure water can be calculated using Equations 2 and 3, respectively.

$$p_s = \chi_w a_w p_v \tag{1}$$

$$a_w = 1 - 0.5\chi_{NaCl} - 10^2_{NaCl} \tag{2}$$

$$p_v = \exp^{\frac{A-B}{C+T}} \tag{3}$$

Where:

p_s is the saturated water vapor pressure of the saline solution
χ_w is the liquid mole fraction of water
a_w is the water activity
p_v is the saturated water vapor pressure of pure water
χ_{NaCl} is the mole fraction of NaCl in the feed solution
A, B, and C are constants with values of 23.1964, 3816.44, and -46.13, respectively

Because saturated water vapor pressure increases exponentially with temperature, it is important to have a high feed temperature to maintain a large gradient. As a result, typical DCMD feed sources have temperatures between 60°C and 90°C.

1.2.2. Temperature Polarization

In DCMD, heat transfer across the boundary layers of the feed and permeate sides is considered to be the most significant limiting factor for mass transfer. Due to the fact that heat is released to the cold permeate as vapor is condensed within the permeate-membrane interface, a temperature gradient is observed within the membrane boundary layers of the feed and permeate sides. This gradient between the bulk fluid temperature and the temperature of the fluid at the membrane surface is termed temperature polarization, as depicted in Figure 1. The magnitude of this limiting factor is calculated from the temperature polarization coefficient (TPC) listed in Equation 4.
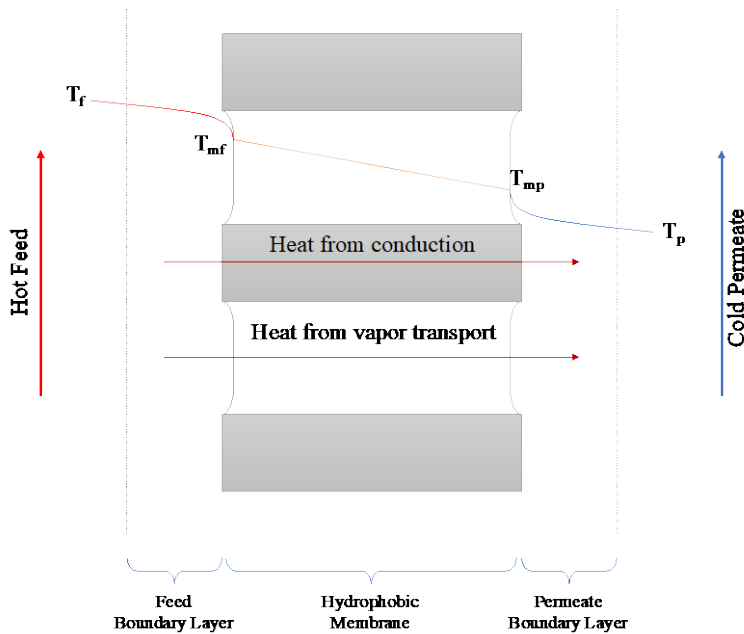
Figure 1. The effect of temperature polarization in DCMD

$$TPC(\Phi) = \frac{T_{fm} - T_{pm}}{T_f - T_p} \qquad (4)$$

Where:
T_{fm} is the membrane surface temperature of the feed
T_{pm} is the membrane surface temperature of the permeate
T_f is the bulk feed temperature
T_p is the bulk permeate temperature

1.2.3. Fouling Potential

Membrane fouling poses the greatest issue when it comes to membrane technologies. Formation of scalants on the membrane surface can significantly diminish overall performance and operational life of a module by clogging pores and changing the physical properties of the membrane related to hydrophobicity and thermal conductivity. Pressure driven processes such

as RO are especially susceptible to fouling because scalants and other contaminants are being forced to the membrane surface. In the case of DCMD systems where the mass transport mechanism is the vapor pressure gradient, fouling propensity is theoretically lower because of the hydrophobic membrane surface. Fouling control methods should still be practiced to mitigate potential surface fouling. Common forms of fouling control include pretreatments and chemical injections in the feed. Pretreatment includes using filters to remove larger particulate matter that has the potential of clogging or damaging the membrane. Additionally, acid or antiscalants can be injected inline on the feed side prior to entering the module to prevent the formation of scalants.

1.2.4. Membrane Characteristics

All MD configurations utilize hydrophobic membranes to create a liquid-vapor interface for mass transport. The membrane's characteristics play a significant role in water flux and overall performance of the system. Such membranes vary in membrane morphology, porometry, thermal conductivity, and liquid entry pressure.

1.2.4.1. Membrane Morphology

Membrane morphology refers to the basic geometry of hollow fiber membranes (HFMs); in particular, the term refers to fiber diameter and membrane thickness. Larger diameter fibers reduce the maximum achievable membrane surface area within a module and, in turn, the water that can be produced. Membrane thickness poses a form of mass transfer resistance and should, therefore, be reduced in order to minimize the path length that vapor has to travel between the feed and permeate side of the membrane. However, exceedingly thin membranes can lead to structural deficiencies and wetting. The optimal membrane thickness was estimated to be 30-60 μm (El-Bourawi et al. 2006). Membrane morphology of hollow fibers is generally determined using scanning electron microscopy (SEM) to observe the cross section (Noor et al. 2018).

1.2.4.2. Membrane Porometry

Porosity, pore size, and pore distribution determine the resistance that vapor experiences as it travels through the membrane. As a result, porometry generally determines a membrane's maximum flux potential and is used in calculating theoretical flux. Membrane porosity (ϵ) refers to the ratio between membrane polymer and the void space within the membrane itself and can be calculated as shown in Equation 5.

$$\epsilon = 1 - \frac{\rho_m}{\rho_{pol}} \tag{5}$$

Where:

ρ_m is the membrane density
ρ_{pol} is the polymer density

Greater flux is generally observed in fibers with high porosity due to the increase in evaporation surface area available for vapor to travel through. MD membranes typically have porosities of 30 to 85 percent and consist of average pore sizes from 100 nm to 1 μm. Increase in pore size also results in increased flux; however, it can also result in a lower liquid entry pressure (LEP) and cause membrane wetting.

1.2.4.3. Thermal Conductivity

The main drawback of the DCMD configuration is that significant heat transfer takes place from conduction through the polymer since both the feed and permeate are in direct contact with the membrane surface. The heat loss on the feed side and subsequent transference to the permeate lowers the VPG due to increased temperature polarization. Therefore, membranes with lower thermal conductivities result in higher observed flux. Membrane thermal conductivity takes into account the conductivity of the membrane polymer and the gas trapped within the pores. The isostrain model shown in Equation 6 is generally used in the literature to estimate the membrane thermal conductivity. However, recent studies showed that the isostress model shown in Equation 7 is a better predictor; this model was adopted for this project (Phattaranawik et al. 2003; Huang and Reprogle 2019).

$$k_m = (1 - \epsilon)k_{pol} + \epsilon k_g \qquad (6)$$

$$k_m = \left(\frac{\epsilon}{k_g} + \frac{1-\epsilon}{k_{pol}}\right)^{-1} \qquad (7)$$

Where:
    k_m is thermal conductivity of the membrane
    k_{pol}, is thermal conductivity of the membrane polymer
    k_g is thermal conductivity of the gas trapped in the pores
    ϵ is the membrane porosity

1.2.4.4. Liquid Entry Pressure

Liquid entry pressure (LEP) is defined as the interfacial pressure difference that a membrane can withstand before pore wetting is observed, i.e., liquid entering the membrane. If operational system pressures exceed the LEP, module performance can be severely affected; flux would be reduced and salt would begin to penetrate the permeate from the feed water. LEP is a function of pore geometry and membrane hydrophobicity and can be estimated using Equation 8 (Franken et al. 1987).

$$\Delta P = P_f - P_p = \frac{-2B\gamma_l \cos\theta}{r_{max}} \qquad (8)$$

Where:
    P_f and P_p are the feed and permeate hydraulic pressures
    B is the pore geometry coefficient

γ is the surface tension of water
θ is the contact angle of the membrane
r_{max} is the maximum pore size of the membrane

Similar to the calculations of the saturated water vapor pressures for saline solutions where activity of the water had to be taken into consideration, variations of water surface tension for high saline feedwaters must also be accounted for. The impact of salt concentration on water surface tension can be expressed as shown in Equation 9 (Zhang et al. 2010).

$$\gamma_{l,new} = \gamma_l + 1.467c_f \qquad\qquad (9)$$

Where:

$\gamma_{l,\,new}$ is the corrected water surface tension
γ_l is the surface tension for pure water at standard temperature and pressure
c_f is the salt concentration of the feed (g/L)

1.2.5. Module Configurations

The efficiency of module performance is dependent on the ability to evenly distribute flow within the module and reduce the effects of temperature polarization. In DCMD, the feed and permeate are pushed through the module co-currently to reduce heat transfer and maximize overall flux. Higher velocities are also associated with an increase in observed flux. Further improvements on flow conditions within module can be made by variations in flow direction within the shell and packing density.

1.2.5.1. Flow Direction

There are two configurations for flow within DCMD modules: axial flow and radial flow. Axial flow configurations directly inject water into the shell of the module, where it then travels down the length of the fiber to the outlet. In radial flow configuration, the feed enters a perforated tube in the center of the module; a baffle inside the tube, located half-way down the length of the module, directs flow radially outward, down the length of the module, back through the perforated tube on the other side of the baffle, and on to the outlet. The configurations can be seen in Figure 2.
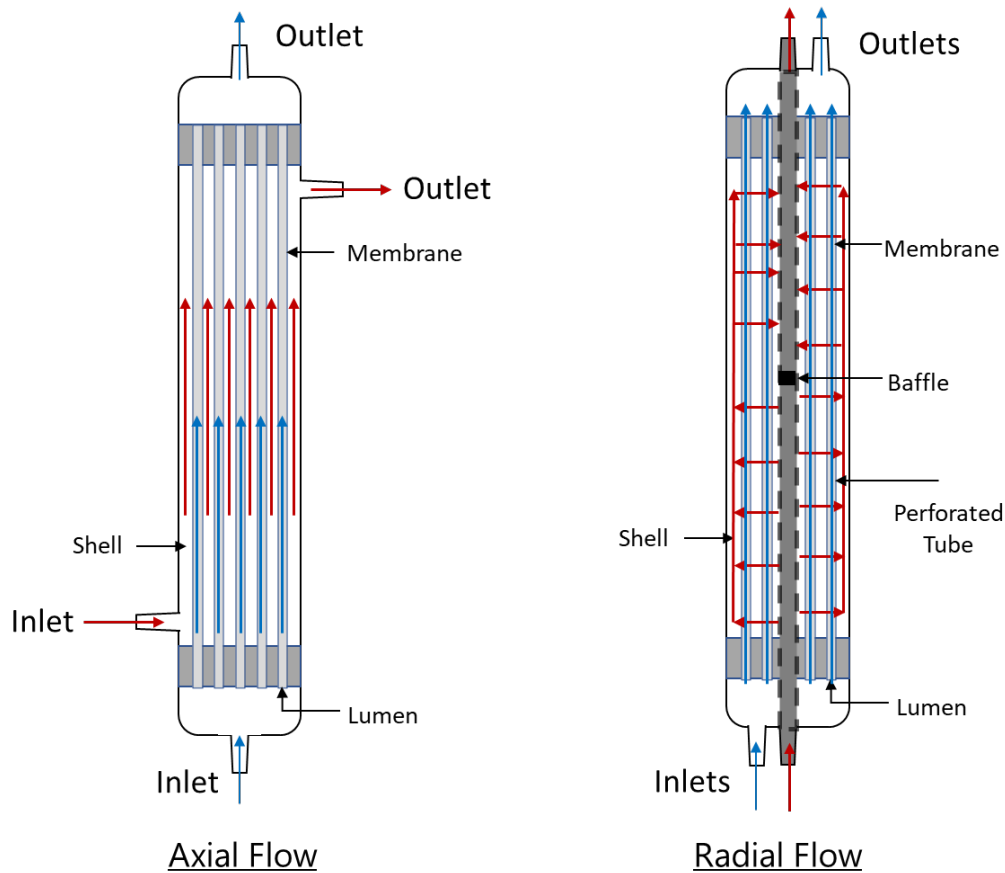
Figure 2. Flow configurations in DCMD modules

Both configurations present their own set of benefits and disadvantages. Axial flow allows for a higher flow velocity because less head is experienced at the inlet and outlet; however, it may not produce the best flow distribution based on the packing density of the fibers. Conversely, radial flow is able to distribute flow more evenly, but at the expense of reducing flow velocity through the module.

1.2.5.2. Packing Density

Packing density refers to the percentage of hollow fibers that are actually in the module versus the maximum number of fibers that can be packed. Studies have shown that higher packing densities lead to lower observed flux due to reduced flow distribution within the module (Huang and Arning 2019). However, overall water production is still greater in highly packed modules because there is more available membrane surface area. Packing density of a DCMD module is determined based on Equation 10.

$$\text{Packing Density (\%)} = \left(\frac{n_f}{n_{max}}\right) \cdot 100\% \qquad (10)$$

Where:

n_f is the total number of fibers in the module

n_{max} is the maxi-mum number of fibers that can fit within a certain diameter module

The maximum number of fibers – circles within a larger circle – can be determined using mathematical software from Packomania or Engineering Toolbox.

1.3. Prior Lab Results

Experimentation was conducted using small-diameter modules and simulated brine (NaCl 5000 mg/L) in lab-scale DCMD systems to collect preliminary data for system modeling. Two types of DCMD HFMs, made of polyvinylidene fluoride (PVDF) and polytetrafluoroethylene (PTFE), were characterized and compared for desalination performance.

1.3.1. Membrane Fabrication and Characterization

The PVDF hollow fiber membranes were fabricated using a dry jet-wet spinning process described in detail elsewhere (Huang et al. 2018). After spinning, the nascent fibers were submerged in deionized water for 24 hours and subsequently freeze-dried to complete post-treatment before usage. The PTFE HFMs fabricated using a melt-extrusion process were acquired from Markel Corporation (Plymouth Meeting, Pennsylvania). Morphologies of the HFMs were characterized using SEM (Hitachi S3200N, Chiyoda-ku, Tokyo, Japan). Pore sizes and distributions were determined using capillary flow porometry (Quantachrome 3G zh, Boynton Beach, Florida). Membrane porosities were estimated using a gravimetric method. Mechanical properties of the fibers were measured at 20°C using a tensile tester (Mark-10 ESM303, Copiague, New York) equipped with a 100 N digital force gauge (Mark-10 Model M5-20, Copiague, New York).

The fabricated PVDF membrane possesses an asymmetric configuration, consisting of an external sponge layer and an internal macro-void layer as shown in Figure 3. During DCMD, hot brackish feed was in contact with the exterior (shell-side) of the HFMs while cold distilled water was in contact with the interior (lumen-side) of the HFMs. The intention was to use the tight pore structure of the sponge layer to prevent the brackish water from intruding into the membranes, and the low tortuosity of the macro-void layer was intended to facilitate water-vapor transport through the membranes. The PTFE membrane has a rather symmetric pore structure as shown in Figure 3. The uni-axial tension applied during the fabrication process created elliptically shaped pores on the external surfaces of the membranes. Table 2 shows the characteristics of the HFMs. The wall thickness of the PTFE membrane is about 1.5 times thicker than that of the PVDF membrane and the associated porosity is about 5/8 of that for the PVDF membrane. Therefore, it was anticipated that the PVDF membrane would produce a higher water flux than the PTFE membrane for a similar pair of inlet temperature in the feed and permeate to the lab-scale DCMD system. The PTFE membrane has a nominal pore size about 1.5 times of that for the PVDF membrane and also possesses a much wider pore-size distribution. This is likely the reason why the values of liquid entry pressure (LEP$_w$) for the two types of membranes are similar at 22°C despite the higher hydrophobicity for PTFE. It is

important to note that LEP$_w$ was observed to decrease with the increase of water temperature and can constrain the operation of DCMD systems at elevated temperatures (Huang et al. 2019). For mechanical properties, the PTFE fiber has a much higher Young's modulus than the PVDF fiber, suggesting that the former is more brittle and has a higher degree of crystallinity. Its failure stress is also substantially higher than that of the PVDF fiber and can facilitate the module-making process.
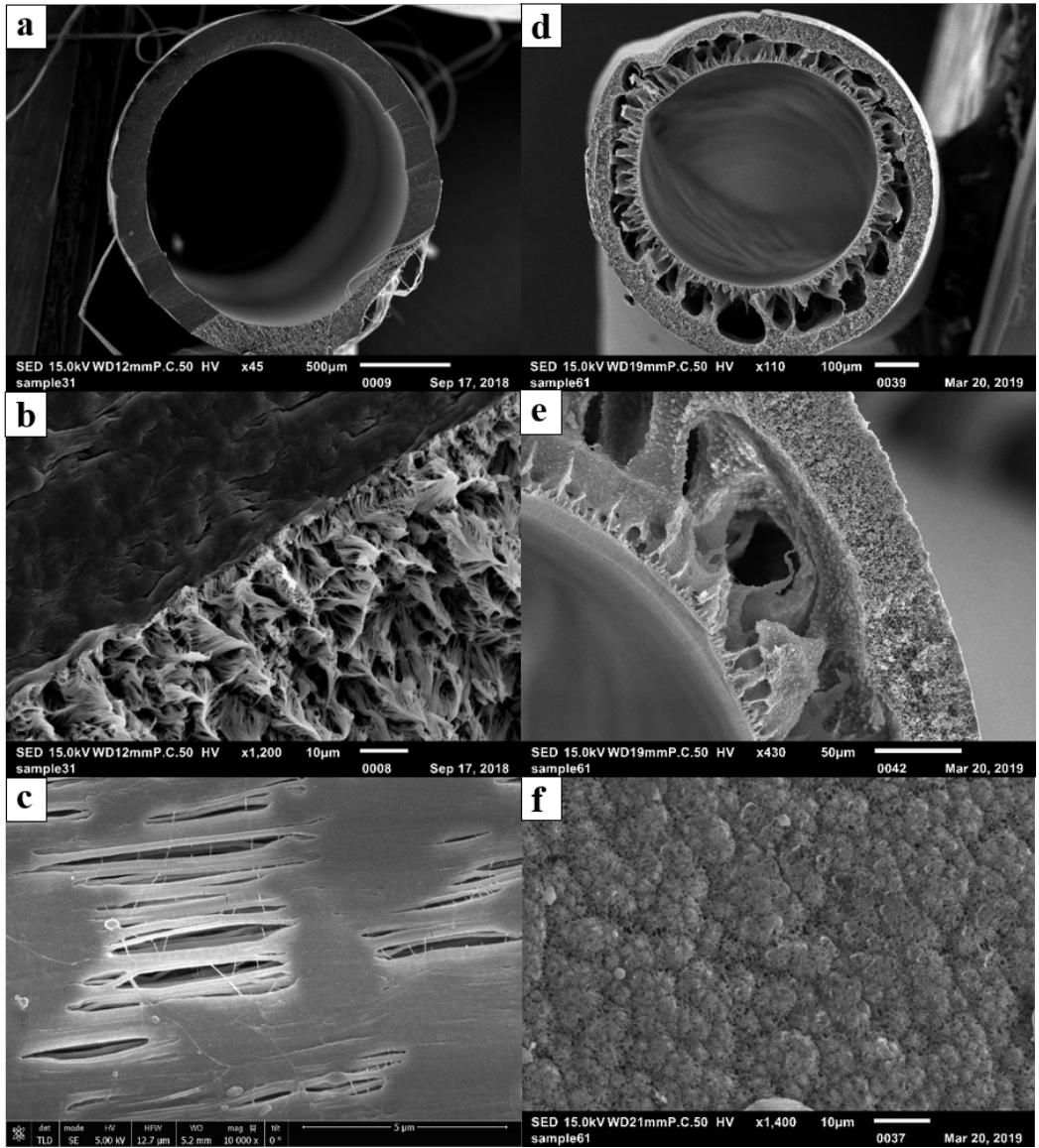
Figure 3. SEM images of the hollow fibers: (a) PTFE fiber, (b) PTFE cross-section, (c) PTFE external surface, (d) PVDF fiber, (e) PVDF cross-section, and (f) PVDF external surface

Table 2. Characteristics of the PVDF and PTFE HFMs

Membrane Characteristic		PVDF	PTFE
Outer diameter (µm) [a]		841±5	1799±50
Wall thickness (µm) [a]		122±22	178±12
Macrovoid to sponge ratio [b]		1.08	N/A
Pore size		0.319/0.333/0.422 [c]	0.385/0.495/0.831 [d]
Porosity		0.79±0.05	0.50±0.04
Failure stress		1.32	>21.5
Young's modulus		15.66	348
Liquid entry pressure, LEP$_w$ (bar)	at 22 °C	1.32	1.37
	at 81 °C	0.53	-

[a] nominal size based on post-processing of SEM images
[b] ratio of the macrovoid-layer thickness to the sponge-layer thickness
[c] minimum pore size/mean pore size/maximum pore size
[d] based on the short axis of the elliptical pore

1.3.2. Module Fabrication

Individual fibers were hand sorted for defects before being fitted inside polycarbonate tubes with an inner diameter of 0.953 cm to achieve fiber packing densities up to 50 percent. Polycarbonate was chosen for its high thermal resistance and good optical clarity. Epoxy resin (Devcon Corporation) was then used to pot each module. The epoxy was cured at room temperature for 24 hours followed by an additional 2–3 hours at 50°C. Prior to use, a section of the cured epoxy was removed from each end of the module to expose the lumen side of the HFMs. Each module underwent a quality assurance/quality control (QA/QC) procedure in the lab after fabrication to check for module integrity before usage.

1.3.3. Laboratory DCMD Experimental Setup

For the lab-scale membrane performance testing, all modules were evaluated in a co-current DCMD configuration with the experimental setup shown in Figure 4. The main objective of the lab-scale study was to quantify water flux and the associated rate of water production per module for the PTFE and PVDF HFMs. The impact of packing density and temperature decline along the module on membrane performance was also investigated. Three packing densities, 10 percent, 25 percent, and 50 percent, were employed for PTFE and PVDF modules. For all the testing, the feed-side and permeate-side fluid velocities were maintained at 0.06 m/s and 0.2 m/s respectively, regardless of the fiber packing density. The intent was to maintain the same level of temperature polarization at the membrane surfaces for data comparison. The temperature polarization (TP) is defined as the temperature difference between the bulk stream and the membrane surface and is a strong function of the fluid velocity. Severe TP can limit the availability of thermal energy in the hot feed for membrane distillation, leading to reduced water flux. For the effect of temperature decline along the module length, the water-flux values generated for PVDF modules with effective fiber lengths of 9 cm and 24 cm were compared. A minimum of three membrane modules per packing density were evaluated to account for variance in operating conditions and fabrication consistency. Sodium chloride solution with a

total dissolved solids (TDS) concentration of 5000 mg/L was used as the feed for the modules. To maintain a constant feed concentration as permeate was generated, deionized water was dripped from a supplementing reservoir into the feed reservoir to make up the loss. Hot brackish water was run on the feed (shell) side of the membrane while cool, purified water flowed through the lumen. The cold stream was pumped through a stainless steel heat exchanger (HE) with a peristaltic pump (model: 77800-60, Cole-Parmer, Vernon Hills, Illinois) before entering the permeate (lumen) side of a module. The hot stream was pumped through the shell-side of a module with a rotary piston pump (model Q, FMI, Syosset, New York) and the feed temperature was controlled using a hot water bath (model: 2335, Fisher Scientific, Hampton, New Hampshire). Flow rates through a module were monitored with rotameters (Cole-Parmer, model T-03219-31). Condensate generated in the lumen was collected in a permeate reservoir, then recirculated into the module. The permeate reservoir was placed on a balance and cumulative mass was measured over time to estimate water flux. Temperature and mass were measured and recorded at 5-minute intervals for the duration of the test. Water samples from the feed and permeate were taken periodically to measure the conductivity of both streams with conductivity cells (Cole-Parmer, $K = 10$ and 0.1, 10 kΩ ATC). For each VPG, the test was run for at least 45 hours after an equilibration period.
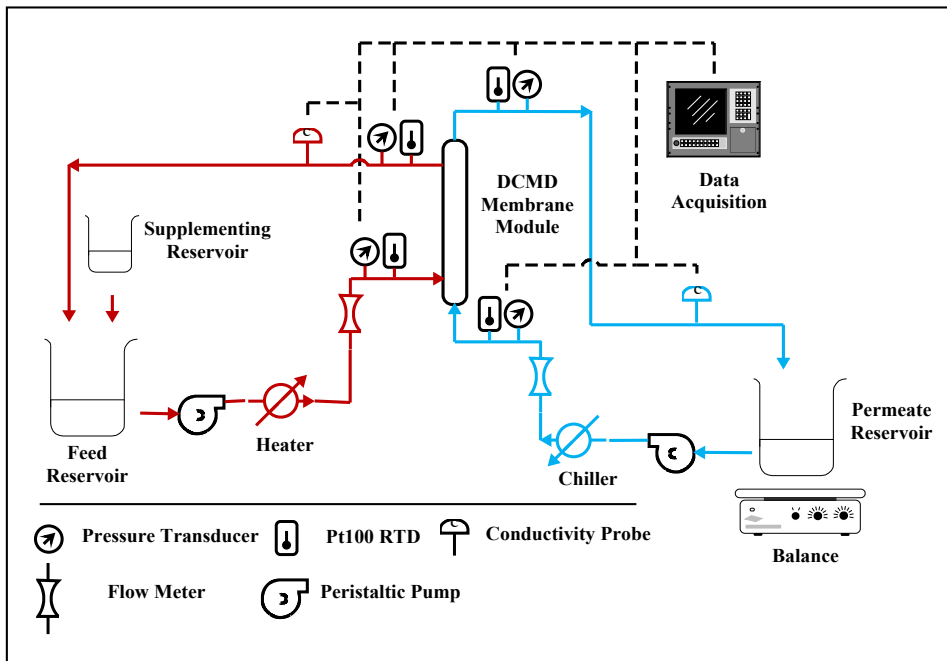
Figure 4. The lab-scale experimental setup for DCMD

1.3.4. Lab-Scale Membrane Performance

Water flux of the membrane modules at packing densities of 10, 25, and 50 percent was measured as a function of the average water-vapor pressure gradient imposed on the modules (Huang and Arning 2019). Since the vapor pressure gradient is the driving force for water diffusion across the membranes, it was observed to scale linearly with the water flux for a specific packing density. Figure 5 shows the correlations for PTFE membrane modules with an

effective fiber length of 9 cm. The membrane surface area for a 10 percent packed module was about 0.0011 m^2 and increased proportionally with packing density. As the packing density increased, the observed water flux declined. This reduction of water flux was probably attributed to the decline of the total heat flow into the module while maintaining the average shell-side fluid velocity. Randomly-packed hollow fibers with an increasing packing density could also result in progressively uneven distribution of fluid flow and thus heat flow among the fibers. A similar trend with packing density was also observed for the PVDF membrane modules. For a 10 percent packing density, the PVDF-based modules had about 0.00264 m^2 of membrane surface area per module. Figure 6 presents a performance comparison between the PTFE and PVDF membrane modules at an average vapor pressure gradient of 1 MPa/cm (e.g., hot inlet: 55–60°C and cold inlet: 22–25°C). For low packing density (i.e., 10 percent) when the thermal energy for distillation is abundant, the PVDF modules exhibited a significantly higher water flux (approximately 1.6 times) than the PTFE module due to the larger membrane surface area per module. However, as the packing density increased from 10 percent to 50 percent, similar water flux was observed for both types of modules while the ratio of the membrane surface area between PVDF and PTFE remained about the same at 2.5. This convergence of observed water flux at high packing density was likely in part due to the lack of thermal energy for distillation as the total membrane surface area in a module grew. Nevertheless, the module water production rate for the PVDF membranes was still 2.5 times of that for the PTFE membranes at 50 percent packing density. This result signifies the importance of reducing fiber diameter in maximizing the water production rate per module for DCMD.
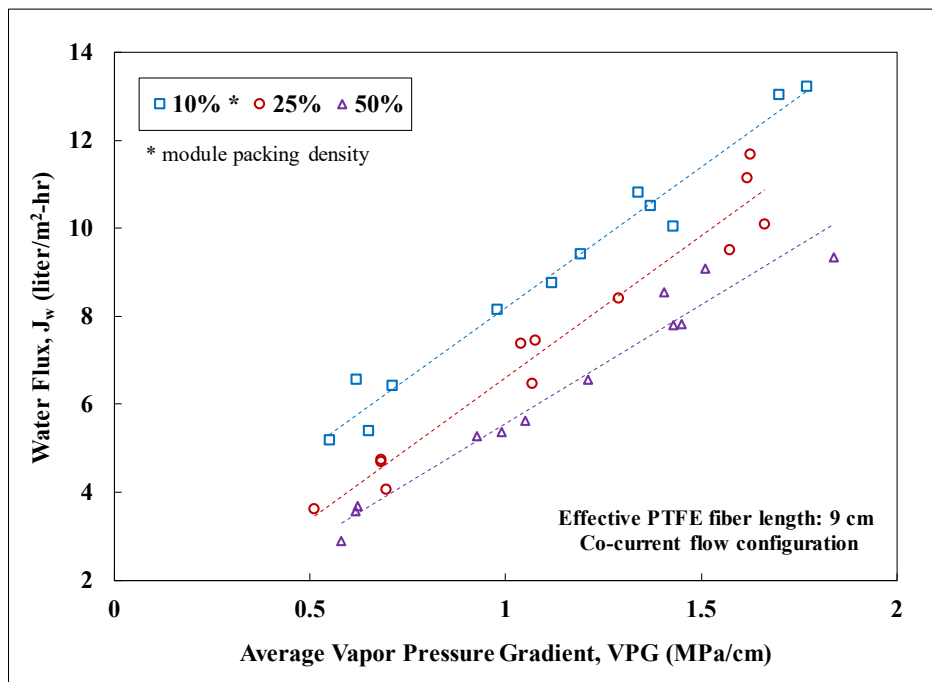
Figure 5. Water flux as a function of the average water-vapor pressure gradient for 10 percent, 25 percent, and 50 percent module packing densities in PTFE membrane modules
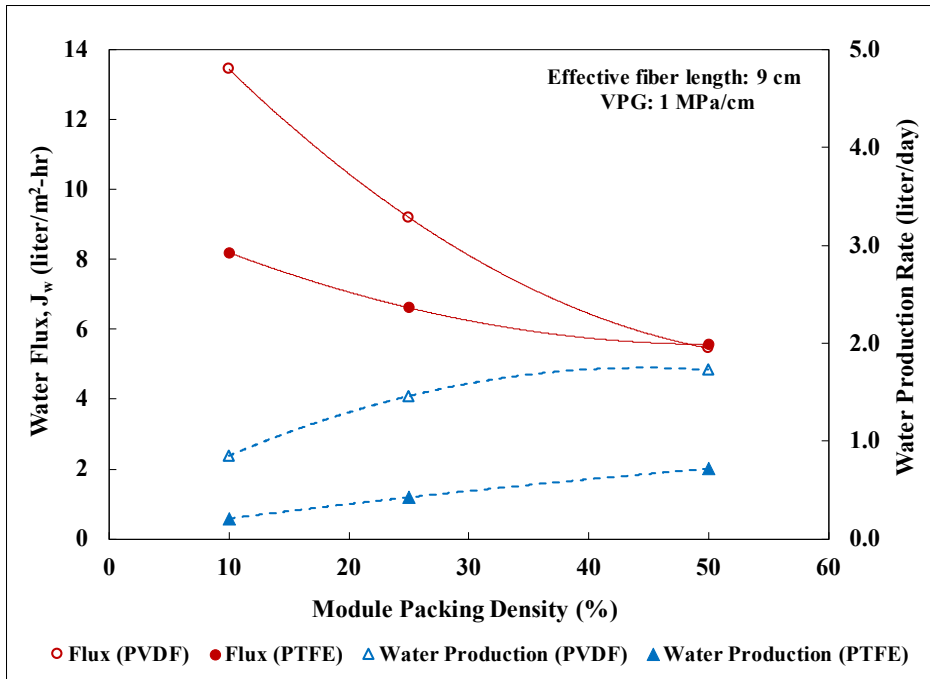
Figure 6. Module performance in water flux and production rate for PTFE and PVDF hollow fiber membranes as a function of packing density at a vapor pressure gradient of 1 MPa/cm

2. Technical Approach and Scope of Work

2.1. Design and Construction of Pilot Plant

2.1.1. Process and Instrumentation

The inherent simplicity of the DCMD configuration has made it the most common form of MD implemented for research and industrial applications. The biggest advantage of the configuration is that a condenser is not required for operation, allowing energy input to remain minimal. Additionally, it requires only basic equipment to operate and is still able to produce relatively high flux. The DCMD process and instrumentation diagram for this study is shown in Figure 7.
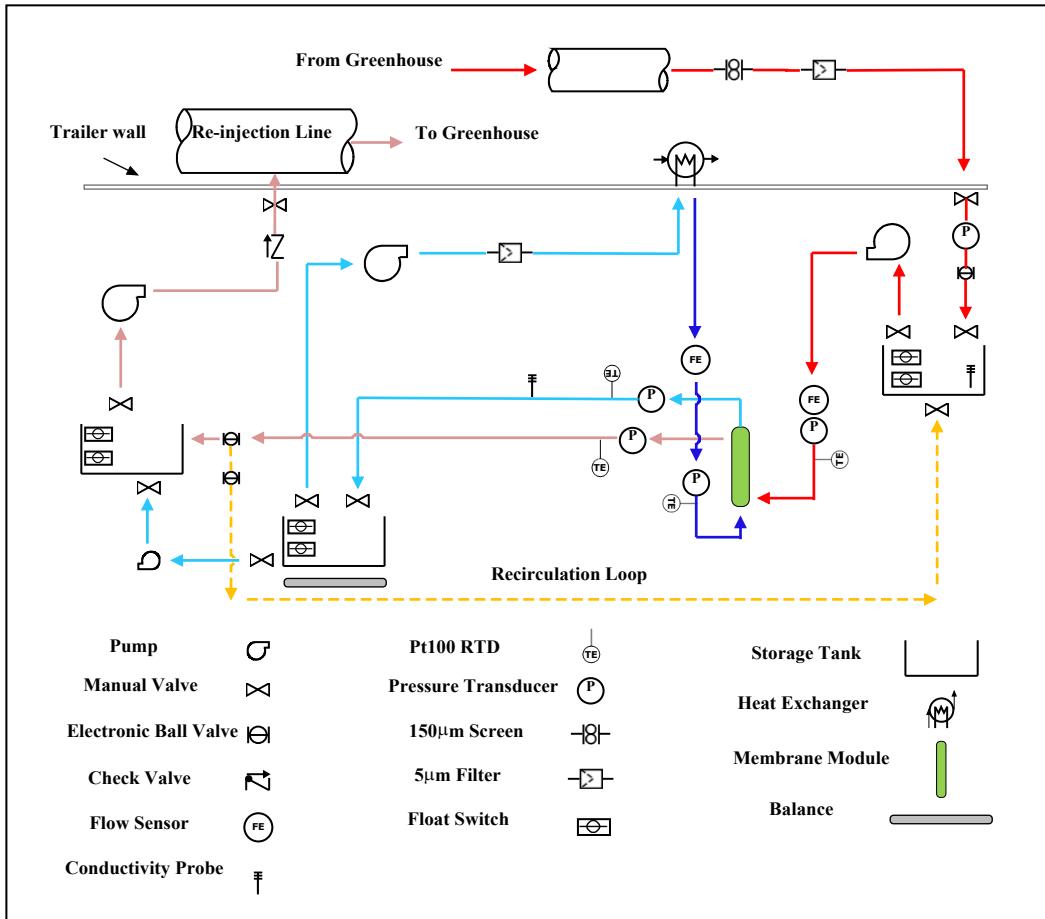
Figure 7. Piping and instrumentation diagram of the pilot-scale DCMD system

The system was constructed inside a 19.8- by 8.5- by 8.5-foot trailer and consisted of two primary process loops: a hot-feed side and cold-permeate side. The feed loop began at the geothermal source and passed through a 150-um stainless steel screen prior to reaching the trailer. This was done to remove larger particulate matter that could potentially damage the membranes or pumping equipment. Once inside the trailer, the feed water filled a reservoir tank – designated as the feed tank – to provide consistent suction head for pumping through the system. A multistage, centrifugal pump (Grundfos CR1S-6 with 0.5-hp motor) was used to pump the feed water through the module to the discharge reservoir (discharge tank). From there, another multistage, centrifugal pump (CR 3-5 with 0.75-hp motor) was used to reinject the concentrate back to the source. In order to prevent fouling from the feed water, the feed loop was equipped with a positive displacement dosing pump (Pulsatron 0.1-12 gallons per day) that would inject acid inline prior to feed water entering the module.

The permeate loop was equipped with a single reservoir, labeled the permeate tank. The tank was placed on a mass balance (Adam Equipment CPWPLUS 200M) to measure water production rate. A single, multistage centrifugal pump (Grundfos CR1S-6 with 0.5-hp motor) was used to pump water through the loop. Beginning at the permeate tank reservoir, water was pumped through an air-cooled HE (2 Row Dual-Core Aluminum Radiator) located outside the trailer. After passing through the HE, particulate matter was removed from the line using a 5-um

membrane filter. The permeate was then pumped through the module and back to the permeate tank. Once enough water was produced to fill the tank, a submersible pump (Active Aqua Submersible Pump 40 gallons per minute (gpm) would drain the produced permeate water into the discharge tank.

Feed water temperature had the potential of reaching 80-85°C; therefore, materials used for construction of the system, in particular the feed loop, were rated for high temperature liquids (>95°C). Schedule-80 chlorinated polyvinylchloride (CPVC) tubes and fittings were used for a majority of the piping requirements for the system; high temperature flex hose was used as an alternative in areas where rigid pipe was not ideal. The piping running from the source to the trailer was wrapped in insulation to prevent heat loss. The three reservoir tanks were made of polyethylene and had 30-gallon capacities.

In addition to having to withstand high temperatures, the instrumentation used in the system had to be corrosion resistant from the high salinity feed water. As a result, a majority of the sensors used were constructed of stainless steel, unless a cost-effective plastic alternative was available. Pressure transducers (Cole-Parmer EW-68074-08), resistive temperature detectors (RTDs, Auber Instruments PT-100), flow transmitters (McMaster-Carr 9687K11), and conductivity meters (Cole-Parmer EW-19500-67 Probe with Cole-Parmer Cond/TDS 500 microcomputer) were used to monitor operating conditions of the system. Float switches (Cole-Parmer EW-07187-24) and electronic ball valves (US Solid 24VDC NC) were used for system automation. Images of the completed pilot-scale DCMC system are provided in Appendix A.

2.1.2. System Autonomy

An integral part of this field study was to develop a completely autonomous and remotely accessible system. The system had to be able to control pump operation, acid dosing, and flow paths based on sensor feedback, as well as have the ability to be shut off remotely. Additionally, recorded data had to be remotely accessible at any time.

2.1.2.1. Logic Control

A Field Programmable Gate Array (FPGA; NI cRIO 9035) logic controller was used in the automation of the DCMD system. Instrumentation control and communication was conducted through integration of 24-VDC digital and analog signal modules (NI 9205, 9217, 9425, 9476 C-Series modules with respective BiRIO wiring interfaces) with the FPGA. The LabVIEW development environment was used to program the FPGA and design the logic control for system automation.

Float switches and pressure transducers were the primary sources of system feedback used to develop the Boolean logic control. Float switches were used to indicate water levels (high or low) inside the three reservoir tanks. Their positions, in turn, determined when valves and pumps needed to be activated. The pressure transducers provided information about the operating pressures at the source inlet and the feed and permeate inlets to the module to determine if safety protocols needed to be initiated. A low source pressure indicated that no water was being provided to the system; as a result, this initiated recirculation to prevent the

pumps from running dry and potentially damaging the pump and/or module. The pressures at the module inlets determined the transmembrane pressure inside the module. If this pressure difference exceeded the LEP, the system would shutdown to prevent damaging the membrane fibers inside the module. Additionally, the module had a maximum operating pressure of 2 bar (29 psi), as specified by the manufacturer, so the system was set to shut down if the system pressure of either loop exceeded 25 psi. Logic flow for the system is shown in Figure 8.

2.1.2.2. Remote Control and Data Acquisition

Due to the fact that the system would be deployed at a remote location, it was imperative the system have the ability to be remotely controlled from anywhere. To achieve this capability, the FPGA was connected to a cellular network-based router (Cradlepoint IBR1100 series). This allowed the control system to be accessed wirelessly by a computer on the same network. A laptop was left on-site to interface with the FPGA. Google Remote Desktop was then used to securely and remotely access the laptop and control the system. Connection could be established from any phone, tablet, or computer that had internet access.

LabView was also used to read and write data to a text file and save the document to the integrated memory of the NI cRIO Controller. As a result, the data could also be accessed remotely at any time. Data were taken in intervals of 15 minutes, with new text files being generated every 12 hours.
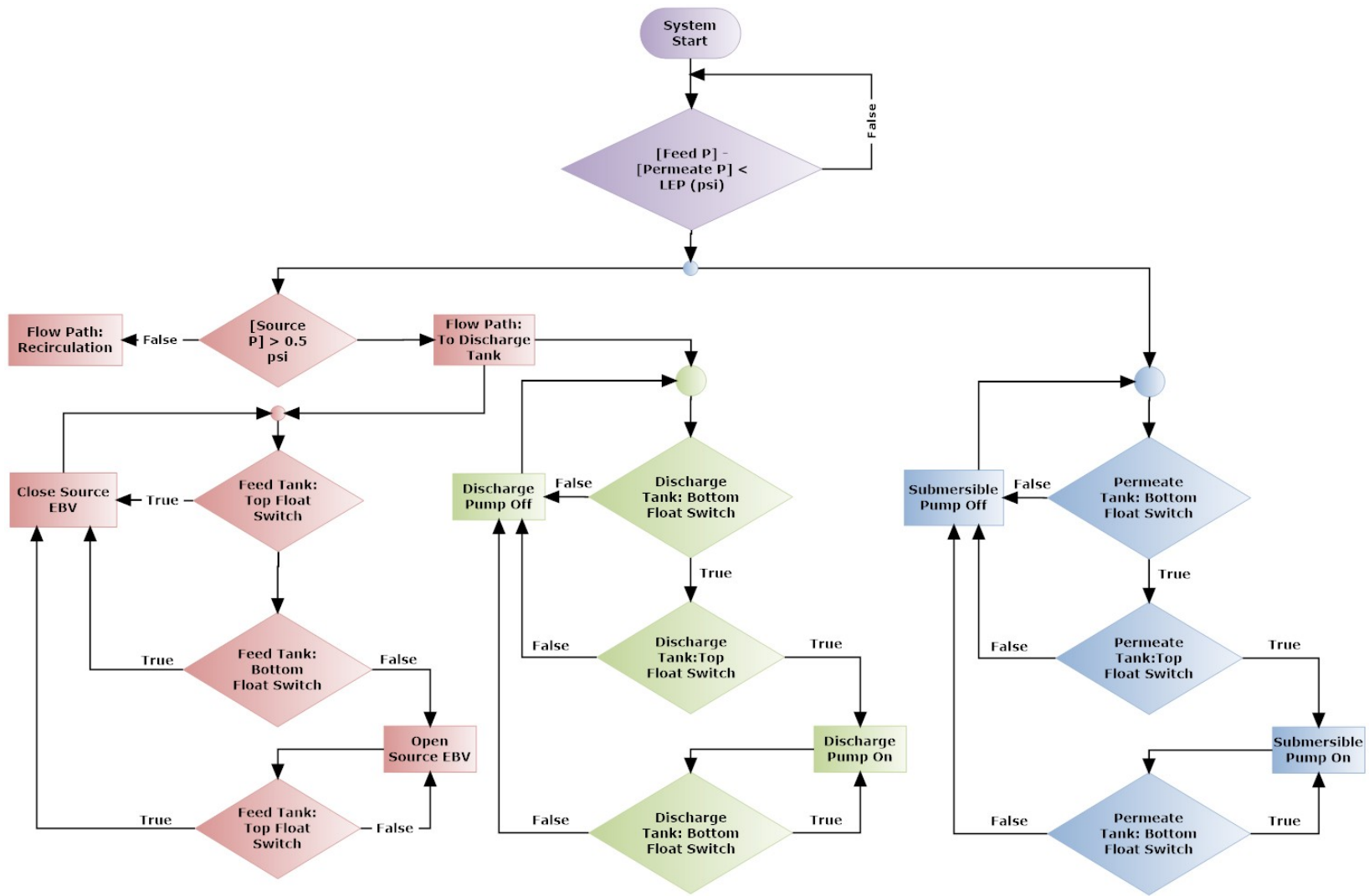
Figure 8. Control logic of the pilot-scale DCMD system

2.2. Field Deployment

2.2.1. Field Site

Masson Farms was selected as the field testing site for the pilot-scale DCMD system. The facility, located in Radium Springs, New Mexico, is the second largest geothermally heated industrial greenhouse in the U.S. A geothermal well provides the majority of heat for the greenhouse at a flow rate of about 1,200 gpm. The geothermal water is circulated through plate and frame HEs that transfer heat from the geothermal stream to a recirculating freshwater stream for space heating. The cooled geothermal water is then pumped back into the rhyolite dike reservoir downstream. Many of the plant species grown at the greenhouse are extremely sensitive to the salt concentration in water. Therefore, water from permitted freshwater wells and the Rio Grande River must be treated to reduce TDS from 1,800 to 300-400 mg/L before it may be used for irrigation. Currently, the greenhouse relies on RO to produce 160 gpm of permeate. Chemical treatment is applied to the feed water for inorganic fouling control, which increases the energy footprint and operating cost of the greenhouse. The intent of this project is to use the cooled geothermal water as the source water of the pilot-scale DCMD system, which utilizes the residual innate heat to produce distilled water for irrigation. Table 3 lists the water quality data of the geothermal fluid from the old and new wells, as well as for the fresh water used for irrigation (Huang et al. 2018). The old geothermal well was decommissioned in 2019 due to calcification of the well casing.

Table 3. Water quality of the geothermal and irrigation fluids

Parameter [a]	Geothermal (old)	Geothermal (new)	Irrigation [b]
Ca^{2+}	114	122	181
Mg^{2+}	11.4	12.1	35.4
K^+	165	151	12.6
Na^+	1,110	1,060	375
Li^+	1.22	na [c]	na
Fe^{2+}	0.5	0.7	na
Sr^{2+}	2.14	2.14	1.9
F^-	5.4	5.4	0.9
Cl^-	1,740	1,590	320
SO_4^{2-}	265	270	619
HCO_3^-	408	401	454
B	0.9	na	na
Si (as SiO_2)	88.1	75.4	38.5
pH	6.6	6.9	8.1
TDS	3,710	3,500	1,850
Temperature (°C)	92	84	20

[a] Units are in mg/L unless otherwise noted
[b] Without treatment
[c] Not available

2.2.2. Preliminary System Check

Prior to the deployment of the pilot plant, a series of system checks was performed in order to verify that all equipment and instrumentation was properly constructed, installed, and functioning. Extensive leak tests were performed on all reservoir tanks, piping, and piping connections; this was especially important for the acid dosing set-up, which could have created hazardous working environments if leaks were present. Sensor and logic control tests were performed to ensure accurate communication between instrumentation and the FPGA, and to confirm that system automation was working correctly. Such tests were performed prior to deployment to minimize troubleshooting on-site.

2.2.3. Field Setup

Prior to deployment, a plan was created to outline the resources that would be provided by the greenhouse and list the demands set forth by greenhouse officials regarding placement of the pilot plant. The greenhouse provided a 240V, three-phase, 60A electrical hookup for powering the system in the trailer. The three-phase power source was converted to single phase for compatibility with equipment and instrumentation.

The greenhouse provided brackish water by tapping into their geothermal water line located at the inlet to the plate and frame HEs. This provided brackish water at source temperature and allowed for the greatest potential vapor pressure gradient to be obtained. Additionally, a second tap was installed at the HE outlet line to serve as a port to reinject the concentrate from the DCMD system back into the geothermal well. Water from the greenhouse's RO system was also provided to fill the permeate reservoir for initial startup of the system.

2.3. Experimental Methods

2.3.1. Flow Configurations

DCMD systems require that the feed and permeate loops pass through the module co-currently in order to maintain the largest possible VPG through the length of the module. Two variations of co-current flow configurations were tested in this study. The first configuration ran the feed water on the shell side of the module and the permeate on the lumen. This was done to maximize the surface area available for vapor to pass through and minimize the risk of plugging the lumen from constituents in the feed water. Conversely, the second configuration ran feed water on the lumen side with the intention of increasing the range of feed flow rate through the module without exceeding the LEP or maximum system pressure. It was hypothesized that a higher flow rate would generate a higher average VPG across the module, which, in turn, would result in higher observed flux. Additionally, a higher flow rate would reduce fouling propensity of a tightly packed shell.

2.3.2. Operating Conditions

Preliminary pressure tests were performed for each module in order to determine a range of flow rates for conducting experiments. System pressure of the modules was considered the limiting factor when determining the operating matrix. The maximum system pressure that the module could withstand was 2 bar (29 psi), as defined by the manufacturer's specifications. This pressure was used to determine the maximum operating flow rates on the shell and lumen sides of the module. A testing matrix was then developed based on the results of the pressure tests; relevant information is provided in Table 4.

Table 4. Experimental design of the pilot testing

Operating Parameter		High	Low
Temperature (°C)	Feed	80	55
	Permeate	40	25
Flow Velocity (m/s)	Feed	0.22	0.08
	Permeate	0.14	0.09

The testing matrix also included a range of temperatures to be tested. However, temperature of the feed was dependent on what was provided by the geothermal well, and permeate temperature was dependent on the ambient temperature since the loop was air cooled. Therefore, the temperatures reflect potential values that could have been experienced from changes in well operation and weather.

2.3.3. Fouling Control and Prevention

Inorganic fouling, specifically from calcium carbonate, could drastically inhibit module performance and reduce operating life. Calcium carbonate is a retrograde soluble compound, meaning that its solubility is reduced with an increase in temperature. This was concerning due to the fact that higher feed temperatures are required for optimal performance in geothermal DCMD systems. Therefore, two forms of fouling control were tested to determine their effectiveness in extending module life. One involved utilizing a high frequency vibrator (Concrete Vibrator 30W Single Phase 3600rpm) attached directly to the module in order to prevent any particulate matter from adhering to the membrane surface and clogging pores. As a more drastic measure, 32 weight percent (wt%) hydrochloric acid was injected inline to lower the pH of the feed and prevent precipitates such as calcium carbonate and ferric hydroxide from forming. These methods were compared to tests conducted without any implementation of fouling control to determine the necessity of such measures.

2.4. Performance Model Development

A MATLAB program was developed to predict the performance of DCMD modules for implementation in techno-economic models of large scale DCMD systems. Model output parameters included average water flux, feed and permeate outlet temperatures, and system pressures.

2.4.1. Coding Approach

The program was designed so that performance predictions could be made with limited user input data. User inputs were broken down into two tiers; Tier 1 information represented the minimum amount of information that the user needed to provide; Tier 2 information represented default model inputs that users could override if the information was available. Tier 1 inputs included module geometry and operational conditions of the feed and permeate loops. Tier 2 information defined the membrane characteristics of the hollow fibers as outlined in the literature review: porosity, pore diameter, wall thickness, thermal conductivity, and fiber outer diameter. Once user inputs were defined, the program supplied all other necessary information required to begin modeling. This included bulk fluid properties, initial guesses, and model execution conditions. Additionally, the module was divided into 1-cm segments for model calculations.

The numerical method of successive substitution was employed in order to predict module performance; the model would continue to perform iterations until the difference between the calculated flux of two consecutive iterations was less than $1 * 10^{-12} \frac{kg}{m^2 s}$.

The first step involved providing the input parameters for calculations; these include the membrane characteristics and operational conditions of the system, as they were either known or user defined. In addition, some initial guesses of the feed and permeate side membrane surface temperatures, flux, and iterative flux difference were defined; the surface temperatures were assumed to equal the bulk temperatures of the feed and permeate loops; the initial flux guess should be a non-zero number; and the flux difference guess should be greater than that defined for the while loop.

The program will then begin an iterative approach for solving permeate flux. Each iteration begins by reading the flux difference value, dN; if this is greater than the defined tolerance, the program steps into the next line of code. Fluid properties at the membrane surface were then calculated based on the membrane surface temperatures. The heat transfer was then calculated to redefine the membrane surface temperatures. Subsequently, these surface temperatures were used in accordance with the Dusty-Gas model to determine water flux. Once the iterative process was completed, an average flux value for the segment is output and used to determine the bulk fluid temperatures of the following segment. This process is repeated until the heat and mass transfer characteristics of every module segment has been calculated. The model outputs the module water flux averaged across all 1-cm segments of the module, the feed and permeate temperatures calculated in the last segment, the total effective area of the module, and the total water produced per module.

2.4.2. Comparison with Lab and Pilot Data

Model estimations were compared with both lab and pilot-scale experimental data sets to determine the accuracy of the performance predictions. Lab-scale performance data of DCMD modules were obtained from a previous study. Comparison to lab-scale data was primarily used to establish a baseline model. The data were also used to understand the correlation between fiber packing density and effective membrane area. The model parameters determined from the

baseline model were then applied to the performance comparison of pilot-scale modules to determine model accuracy of commercially available modules.

A majority of model tuning was performed with comparison of lab-scale data. As seen in the summary of lab-scale experimental data, modules of three packing densities were studied: 10 percent, 25 percent, and 50 percent. In regard to model tuning, the 10 percent data were used to reasonably adjust membrane characteristic values in the model so that flux and temperature predictions would match with experimental results. The 25 percent and 50 percent data were then used to determine a correlation between packing density and effective surface area of the membranes. This relationship was then applied to determine a rough estimate for the effective area of a pilot-scale module. The effective area coefficient value was then adjusted accordingly to match model predictions with experimental pilot data.

Once the model was finalized, an Excel add-in was generated using MATLAB's Library Compiler extension. This add-in was integrated into an Excel program that performed techno-economic modeling of DCMD systems.

2.5. Techno Economic Model Development

Using the performance outputs given by the DCMD performance add-in, a techno-economic model could then be constructed. The primary goal of the model was to provide an appraisal level cost estimation for large-scale DCMD systems given module performance characteristics, feed water chemistry, equipment fabrication materials, and a desired production rate. The format of the model followed that set in the Reclamation WaTER excel spreadsheet, with inputs for each component input on individual tabs in the spreadsheet and a "Report" tab that included a summary of the recommended equipment sizing and predicted capital and operating and maintenance costs of the large-scale system. The model sizes all major components necessary for a large-scale DCMD facility, which include: microfiltration, acid pretreatment, DCMD modules, air cooled HEs, pH readjustment, concentrate disposal, reservoirs, pumps, and operating and maintenance costs.

The two processes that were unique to this program were the DCMD modules and the air-cooled HEs, as they have not been implemented in other cost estimating programs. The DCMD process tab served as the primary control tab in sizing the system. The performance outputs calculated in this tab with the Excel add-in was used to size other unit operations and operating costs for a large-scale DCMD system.

3. Results and Discussion

3.1. Pilot Experiments

Two DCMD modules purchased from Markel Corporation were used for pilot experiments. The modules were 20 inches in length, 2.5 inches in diameter, and had a packing density of 70 percent. They utilized PTFE HFMs and had a radial flow path. The operational conditions for the pilot experiments differed between the two modules due to flow constraints determined in the pressure tests described previously, and because feed temperature from the well varied throughout the duration of the experiments.

3.1.1. Module 1

The flow configuration for Module 1 ran feed water on the shell side and permeate through the lumen. This maximized the total membrane surface area for the module to 1.3 m^2 and addressed the initial concern of clogging the lumen if the feed was run through that side. The performance test for Module 1 was conducted until it was deemed that the module was "dead" when one of the following conditions occurred: feed flow rate reached 0 gpm; system pressure reached maximum module pressure of 2 bar (29 psi); or pressure differential exceeded LEP. An average feed temperature of 80°C was observed through the duration of the test; permeate temperature fluctuated based on the ambient temperature. Other than the 150-um screen on the feed loop and 5-um filter on the permeate loop, no form of fouling control was installed for the test. Measurements from the test can be seen in Figure 9 and Figure 10.

Figure 9. Feed and permeate inlet temperature and the corresponding VPG of Module 1 over time

Figure 10. Feed and permeate flow rates and the corresponding inlet pressures of Module 1 over time

System pressure and feed flow rate were the primary measurements used to determine the current condition of the module in regard to fouling level. As seen in Figure 11, feed flow rate and pressure were stable at 0.87 gpm and 14 psi, respectively, over a 24-hour period. However, as the test continued, flow rate was observed to decrease drastically and system pressure began to rise. Such observations marked the formation of scalants inside the module. The test was terminated when feed flow reached 0 gpm, which signified complete blockage at the feed inlet of the module.
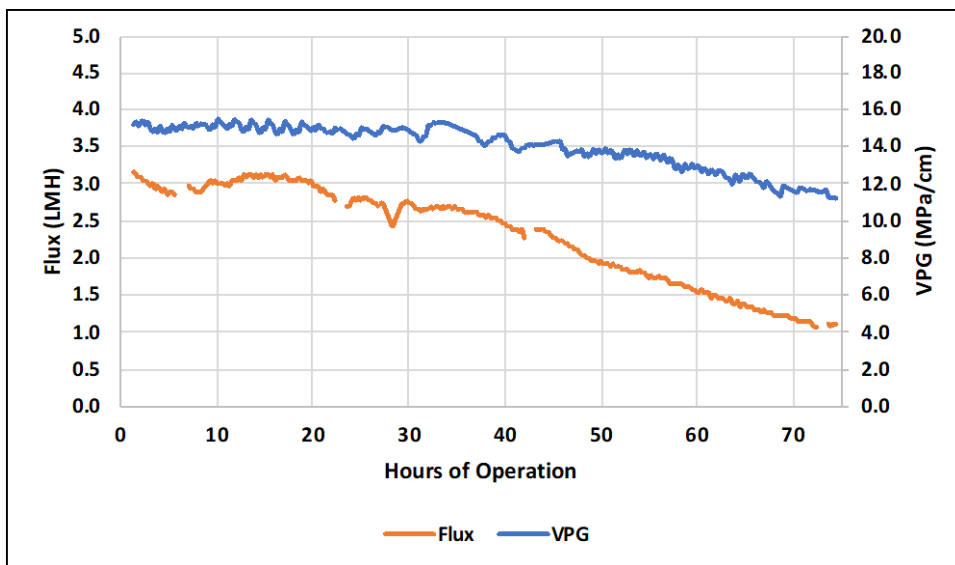
Figure 11. Water flux and the corresponding VPG of Module 1 over time

Water flux was the primary indicator of overall module performance and was calculated based on the accumulated mass over time. Flux depended on the VPG across the module, as it is the main driving force in DCMD systems; the higher the VPG, the greater the observed flux. It was

observed that water flux severely devolved after around 24hours of operation – the point that exhibited the onset of membrane fouling. Scalants had begun to clog the pores of the membrane and prevent water vapor from passing through. As a result of precipitates continuing to form within the shell, feed flow through the module became constricted. This, in turn, severely dropped the VPG due to temperature polarization. When flow rate was lowered from obstructions at the inlet, the residence time of feed water in the reservoir tank increased and subsequently experienced greater heat loss between feed tank refills. This lowered feed inlet temperature and inhibited VPG. The results obtained from Module 1 revealed that integration of additional forms of fouling control such as pH adjustment is necessary to extend module life and performance.

3.1.2. Module 2

To address the fouling observed with Module 1, scalants were analyzed using X-Ray Diffraction (XRD) to determine their chemical compositions. The analysis concluded that calcium carbonate and ferric hydroxide were the primary constituents of membrane fouling. An acid injection system was installed to dose the feed water, inline, to a pH of 4.5 – the pH at which calcium carbonate and ferric hydroxide remain soluble at the feed temperature of 80°C. The flow configuration for Module 2 ran feed water through the lumen and permeate on the shell as an additional fouling control measure; it was believed that the increased feed velocity would reduce fouling propensity and potentially increase water flux. The membrane surface area through the lumen was 1.1 m². Feed water quality had changed for the Module 2 test and required adaptation of a new operational sequence. An increased level of gas bubbles caused de-priming of the multistage centrifugal pump on the feed loop, resulting in the system pressure exceeding LEP and the system being shut down. To combat this problem, the pumps were put on a timer sequence: 30 minutes on, 5 minutes off. Additionally, a DC-powered vent valve was attached to the feed pump and would vent/re-prime during the 5-minute off period. The operational measurements for the test conducted with Module 2 are shown in Figure 12 and Figure 13.
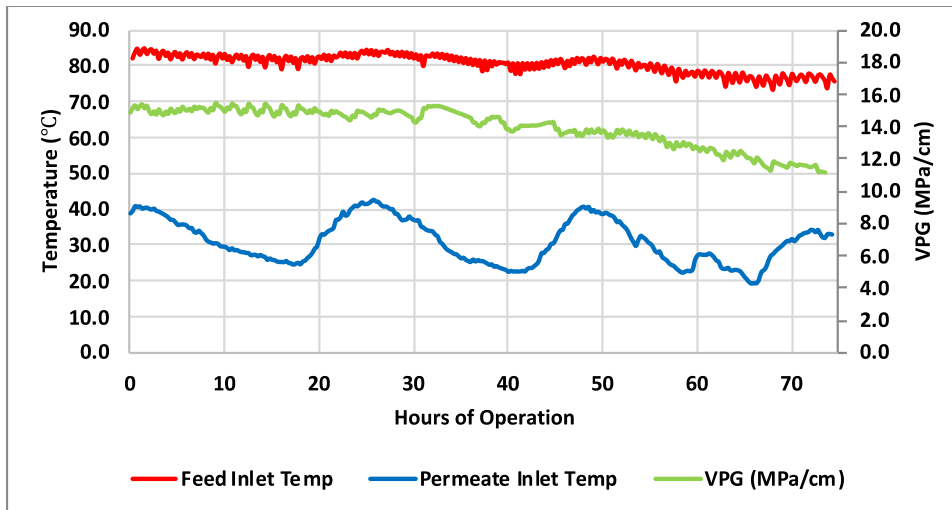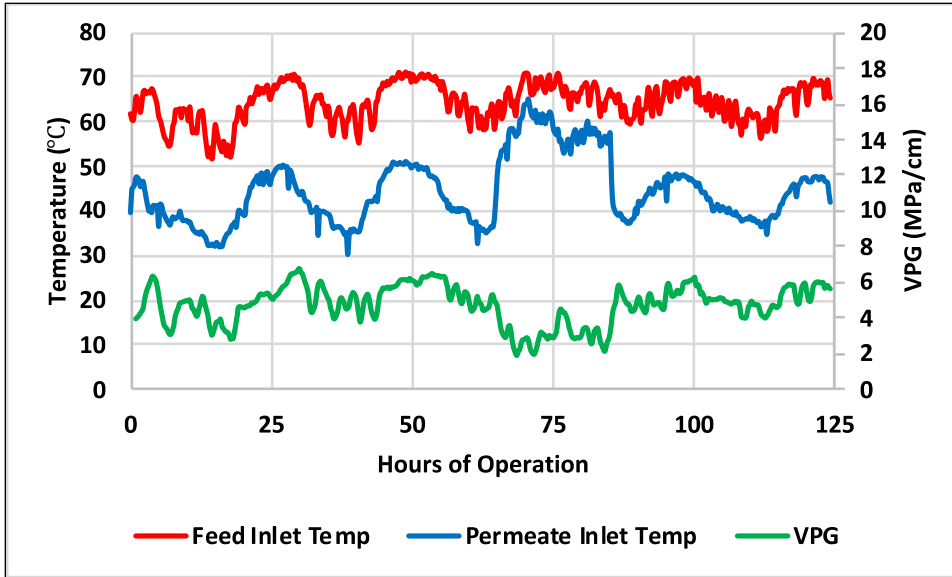
Figure 12. Feed and permeate inlet temperature and the corresponding VPG of Module 2 over time
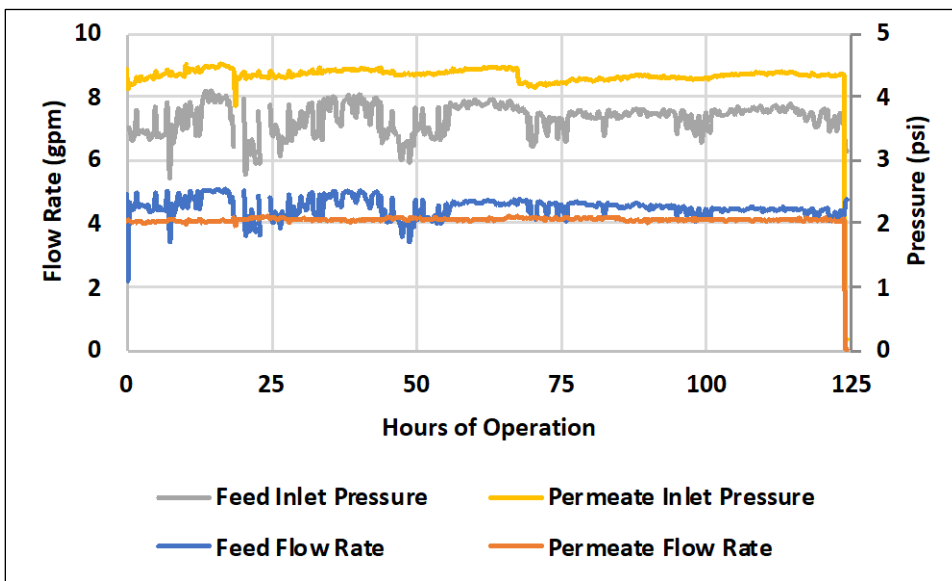
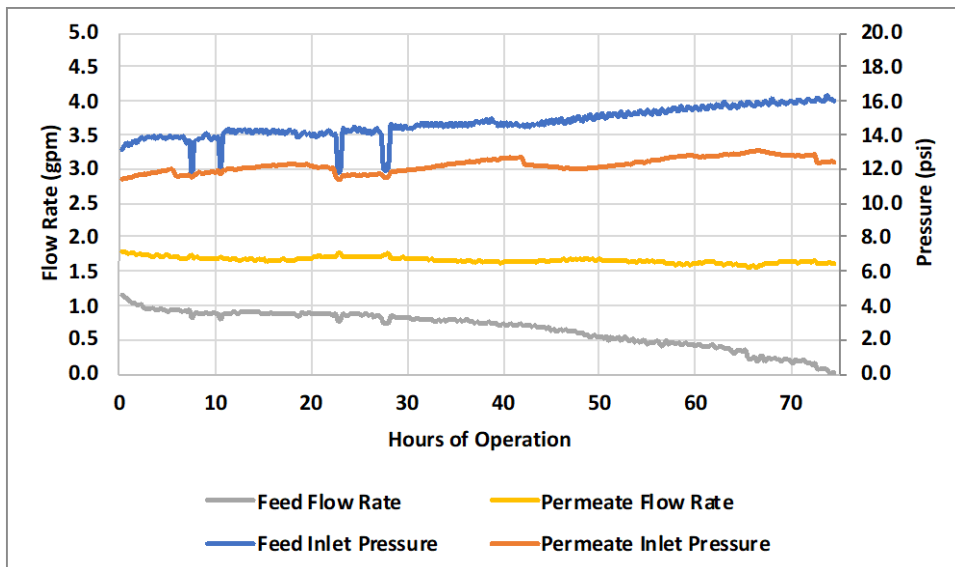Figure 13. Feed and permeate flow rates and the corresponding inlet pressures of Module 2 over time

The effect of gas bubbles on pump performance can be seen in the fluctuation of the feed pressure and flow rate. The sudden drops of pressure and flow rate represent the pump losing prime; the subsequent increase of pressure and flow rate represent the re-stabilization of the system as a result of venting. The relatively constant feed pressure and flow rate indicates that acid injection is an effective method of preventing inorganic fouling inside the module and is able to extend the operating life significantly. The performance results of the test can be seen in Figure 14.
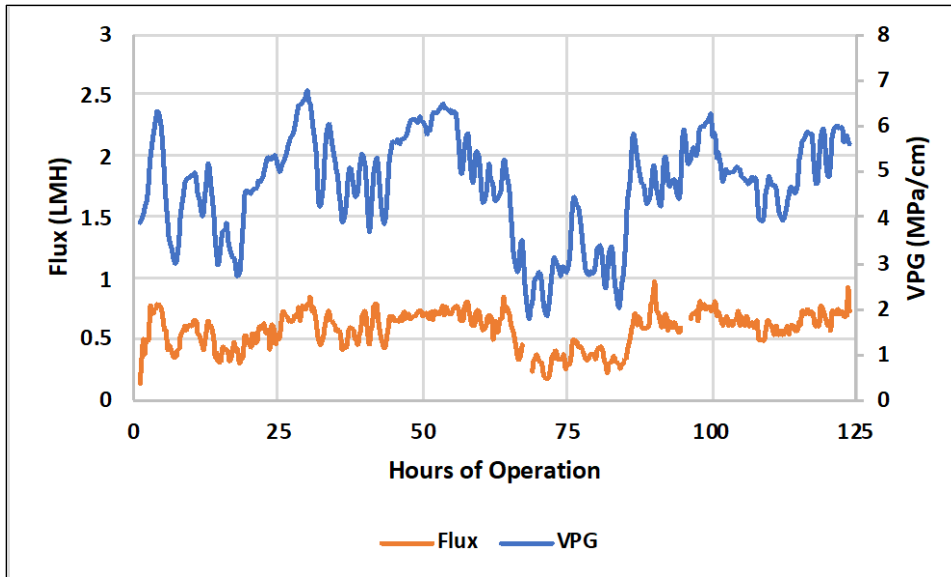
Figure 14. Water flux and the corresponding VPG of Module 2 over time

The VPG is substantially lower when compared to the measurements in the test conducted with Module 1. As a result, the water flux was also observed to be much lower. A reduction in VPG by 50 percent, as compared to Module 1, results in a flux drop that is much greater than 50 percent. These results highlight the importance of a large VPG in DCMD module performance.

3.2. Performance Modeling

The development of a performance model was intended to provide information vital to designing and constructing large-scale DCMD systems. Heat transfer, mass transfer, and system pressure calculations were conducted to accurately model DCMD module performance.

3.2.1. Development

3.2.1.1. Heat Transfer Model

The primary goal of calculating heat transfer was to estimate the surface temperatures on either side of the membrane so that a vapor pressure gradient could be determined for flux predictions. Interfacial temperatures had to be used because DCMD performance is limited by the membrane boundary layers, as expressed by effects of temperature polarization. Consequently, heat transfer through the membrane was modeled by using the conditions of the feed and permeate boundary layers. Membrane surface temperatures on the feed side (T_{fm}) and permeate side (T_{pm}) cannot be measured directly, therefore, they were evaluated using bulk fluid temperatures and local heat transfer coefficients in relations developed based on energy conservation from the feed, through the membrane, to the permeate:

$$T_{fm} = \frac{\frac{k_m}{\delta}\left(T_p + \left(\frac{h_f}{h_p}\right)T_f\right) + h_f T_f - N\Delta H_{LV}}{\frac{k_m}{\delta} + h_f + \frac{k_m h_f}{\delta h_p}} \qquad (11)$$

$$T_{pm} = \frac{\frac{k_m}{\delta}\left(T_f + \left(\frac{h_p}{h_f}\right)T_p\right) + h_p T_p + N\Delta H_{LV}}{\frac{k_m}{\delta} + h_p + \frac{k_m h_p}{\delta h_f}} \qquad (12)$$

Where:

T_f and T_p are the respective bulk fluid temperatures of the feed and permeate sides

N is the flux

ΔHLV is the latent heat of vaporization of water

km is the effective conductivity of the membrane

δ is the thickness of the membrane

h_f and h_p are the feed and permeate heat transfer coefficients, respectively

h_f and h_p were calculated using the correlations of Equations 13 and 14, respectively.

$$h_f = \frac{Nu_f k_f}{d_{h,f}} \qquad (13)$$

$$h_p = \frac{Nu_p k_p}{d_{h,p}} \qquad (14)$$

Where:

k_f and k_p are the feed and permeate water thermal conductivities, respectively

$d_{h,f}$ and $d_{h,p}$ are the hydraulic diameters for the feed and permeate, respectively

Hydraulic diameters for the feed and permeate ($d_{h,f}$ and $d_{h,p}$) were dependent on flow configurations set for operation – different for flow on shell and lumen. The calculation of local heat transfer further required the use of dimensionless numbers to characterize fluid behavior within the membrane boundary layers: Nusselt number (Nu), Graetz number (Gz), Reynolds number (Re), and Prandtl number (Pr). The Nu number represents the ratio of convective to conductive heat transfer within the fluid. There are many correlations for deter-mining Nu; however, the Sieder-Tate correlations are widely used in the modeling of DCMD systems. Such correlations are dependent on laminar or turbulent flow regimes and were determined by employing the Gz number based on Equations 15 and 16.

For Gz>100:

$$Nu = \left(3.66 + \frac{0.668Gz}{1 + 0.04Gz^{2/3}}\right)\left(\frac{\mu_b}{\mu_m}\right)^{0.14} \qquad (15)$$

For Gz<100:

$$Nu = 1.86(Gz)^{1/3}\left(\frac{\mu_b}{\mu_m}\right)^{0.14} \qquad (16)$$

Where:

    μ_b is the bulk fluid viscosity of either the feed or permeate

    μ_m is the viscosity observed at the feed or permeate membrane surface

The Gz number characterizes thermal development in a conduit and employs the Re and Pr numbers as shown in Equations 17 and 18.

$$Gz_f = Re_f Pr_f \frac{d_{h,f}}{L} \tag{17}$$

$$Gz_p = Re_p Pr_p \frac{d_{h,p}}{L} \tag{18}$$

Where:

    L is the length of the module

The Re number is used to characterize flow regime and is the ratio between inertial and viscous forces. The Pr number is a material/fluid property and is the ratio between momentum diffusivity and thermal diffusivity. They are expressed in Equations 19-22.

$$Re_f = \frac{\rho_{m,f} V d_{h,f}}{\mu_{m,f}} \tag{19}$$

$$Re_p = \frac{\rho_{m,p} V d_{h,p}}{\mu_{m,p}} \tag{20}$$

$$Pr_f = \frac{\mu_{m,f} C_{p,f}}{k_f} \tag{21}$$

$$Pr_p = \frac{\mu_{m,p} C_{p,p}}{k_p} \tag{22}$$

Where:

    $\mu_{m,f}$ is the viscosity of the feed at the membrane surface

    $\mu_{m,p}$ is the viscosity of the permeate at the membrane surface

    $C_{p,f}$ and $C_{p,p}$ are the specific heat capacities of water at constant pressure on the feed and permeate sides, respectively

    k_f and k_p are the thermal conductivities of the feed and permeate waters, respectively

Additionally, the surface temperatures were used with the Antoine equation (Equation 1) to determine the vapor pressure on either side of the membrane wall and the associated mass transfer.

3.2.1.2. Mass Transfer

In general, mass transfer in DCMD takes place in the form of water vapor; vapor from the feed is transported through the hydrophobic pore structure of the membrane and condensed in the

permeate. The Dusty-Gas model expressed in the form of Darcy's Law as shown in Equation 27 was applied to estimate water flux across the membrane.

$$N = B_m \Delta P = B_m\left(p_{v,mf} - p_{v,mp}\right) \qquad (27)$$

Where:

N represents flux

B_m is the mass transfer coefficient

$p_{v,mf}$ and $p_{v,mp}$ are the vapor pressures of the feed and permeate waters at the membrane surface, respectively

The mass transfer coefficient was dependent on several membrane characteristics – porosity (e), pore diameter (r_p), tortuosity (τ), membrane thickness (δ), thermal conductivity (k), average membrane temperature (T_m) – and on the dominant mode of diffusion – Knudsen, molecular, or Knudsen-molecular. It was assumed for DCMD modeling that Knudsen-molecular diffusion was the dominant form of mass transport and the mass transfer coefficient was expressed as Equation 28 (Huang and Reprogle 2019).

$$B_m = \frac{1}{RT_m}\left(\frac{D_w^k D_{w-a}^0}{D_{w-a}^0 + P_a D_w^k}\right)\left(\frac{MW}{\delta}\right) \qquad (28)$$

Where:

R is the universal gas constant

MW is the molecular weight of water

D_w^k is the Knudsen diffusion coefficient

D_{w-a}^0 is the pressure-independent molecular diffusion coefficient

The diffusion coefficients are written as Equations 29-30.

$$D_w^k = \frac{2\epsilon r_p}{3\tau}\sqrt{\frac{8RT_m}{\pi MW}} \qquad (29)$$

$$D_{w-a}^0 = 4.46 \cdot 10^{-6}\frac{\epsilon}{\tau}T_m^{2.334} \qquad (30)$$

3.2.1.3. System Pressure Model

It was important to predict system pressure on the shell and lumen of the module in order to determine the flow constraints on either side. The model utilized an empirical equation as shown in Equation 31 for flow in permeable tubes as the base formulation for modeling pressure on the lumen side of the module fibers:

$$\Delta P = \frac{8\mu v_0}{R^2}\left(1 + \frac{v_w L}{v_0 R}\right) \qquad (31)$$

Where:

    μ is the bulk fluid viscosity
    v_0 is the velocity through the tube
    R is the inner radius of the tube
    v_w fluid velocity normal to the tube wall of the membrane (i.e., flux represented as velocity)
    L is the length of the module

The correlation did not take into consideration entrance and exit effects; therefore, an additional head loss coefficient had to be incorporated into the model equation as shown in Equation 32.

$$\Delta P = K\frac{\rho v_0^2}{2} + \frac{8\mu v_0}{R^2}\left(1 + \frac{v_w L}{v_0 R}\right) \qquad (32)$$

Where:

    K is the entrance/exit head loss coefficient for the pilot DCMD module

The value was calculated by substituting the observed lumen pressure drop in pressure tests of the module into the equation and solving for K. The feed and permeate were both at 25°C, so v_w was considered negligible. The calculated coefficients for each test were then plotted to determine a correlation as shown in Equation 33 with respect to velocity through the tube.

$$K = 673.04v_0^{-0.533} \qquad (33)$$

Figure 15 shows the correlation that was developed. K normally represents a constant in fluid mechanics and does not change with operational conditions of a system. This is not the case in calculating this value for DCMD modules; rather, the flexibility of the hollow fibers causes the value of K to vary based on lumen flow rate. As fluid is pumped through the lumen at a higher rate, the fiber expands and reduces the overall head from the module. Since Equation 32 applies to rigid tubes, the derived model seen in Equation 33 is most likely an overestimation of the lumen system pressure.
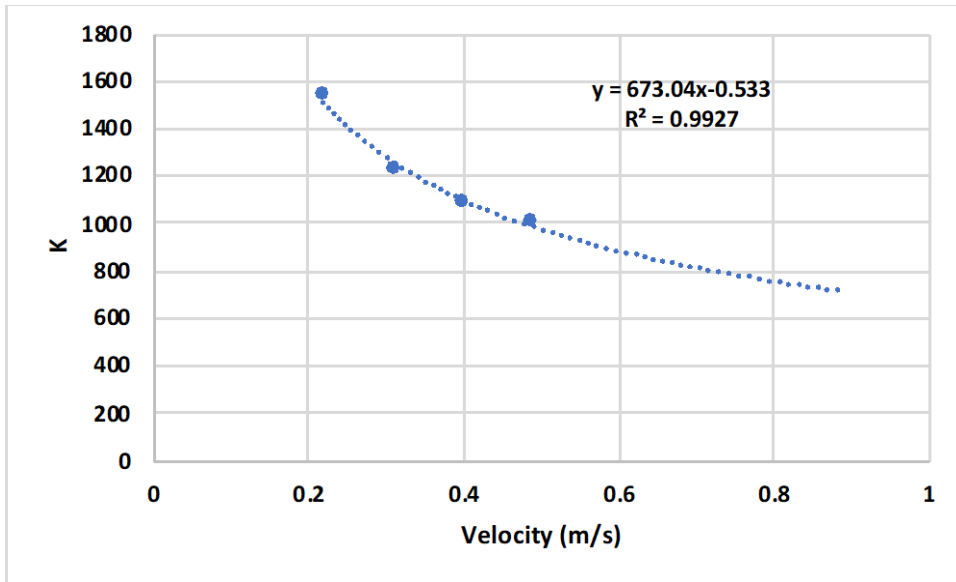
Figure 15. Entrance/exit head loss coefficient for the pilot DCMD module

Unlike lumen pressure, there were no predetermined empirical correlations that could be used to model system pressure on the shell side of module. As a result, a shell pressure correlation was developed using solely experimental pressure test data. Because the membrane fibers are not rigid tubes, the shell pressure was not only dependent on shell velocity, but lumen velocity as well. Polymath was used to develop a non-linear regression in the form of Equation 34.

$$\Delta P = A v_s^2 + B v_l^2 \qquad\qquad (34)$$

Where:

      A and B are regression constants
      v_s and v_l are shell and lumen velocities, respectively

A second order fit was chosen for the regression to comply with the general kinetic energy form: $\frac{1}{2}\rho v^2$. The data used for regression development can be seen in Table 5.

Table 5. Data for modeling of the shell pressure

Shell Velocity (m/s)	Lumen Velocity (m/s)	Shell Pressure (psi)
0.37	0.22	11
0.35	0.31	11.4
0.34	0.40	12
0.30	0.49	12.7

The final regression for modeling shell pressure was determined to be Equation 35.

$$\Delta P = 65 v_s^2 + 25 v_l^2 \qquad\qquad (35)$$

3.2.2. Model Tuning and Verification

Model accuracy was verified by comparison of several performance parameters: flux, feed and permeate output temperatures, and shell and lumen system pressures. Lab-scale data obtained from a previous DCMD study were used to tune the model. Pilot data were then used to further improve model robustness in large-scale DCMD system design applications. The goal of the model was to be able to predict DCMD module performance with a maximum 20 percent error.

3.2.2.1. Flux and temperature Tuning

Two levels of tuning were performed on the model: membrane characteristics and effective surface area. Membrane characteristics have a significant impact on model accuracy; small changes in certain properties can cause major deviations in model predictions. Therefore, it is important to use experimental data to tune such characteristics to their true values. Additionally, the effective membrane surface area of a DCMD module decreases as fiber packing density increases. This is due to degradation of flow distribution within the module and an increase in contact points between fibers. The effective area cannot be directly measured and required the implementation and tuning of an "effective membrane surface area coefficient" (f) to accurately predict module performance of large-scale DCMD modules. The coefficient was a dimensionless factor used to determine the true active surface area of the module and predict permeate flux that represented the average performance of the module, not simply the flux across the active surface; if not used, the model would predict flux values significantly higher than values that would be observed.

In order to tune membrane characteristics, data from experiments conducted with 10 percent packed modules was used. Lab-scale modules with 10 percent packing were ideal for such tuning purposes because it can be assumed that flow is evenly distributed through the length of the module, making the effective membrane surface area 100 percent. Membrane thermal conductivity was considered the primary tuning factor because it had the greatest variability associated with its measured value. The tuning range for the membrane property was 0.045 – 0.25 W/m-K: the calculated effective conductivity to the material conductivity of PTFE. An initial comparison of the model to experimental data was made to form a baseline for accuracy. Deviations from experimental values are shown by plotting model values against experimental results as seen in Figure 16, Figure 17, and Figure 18.
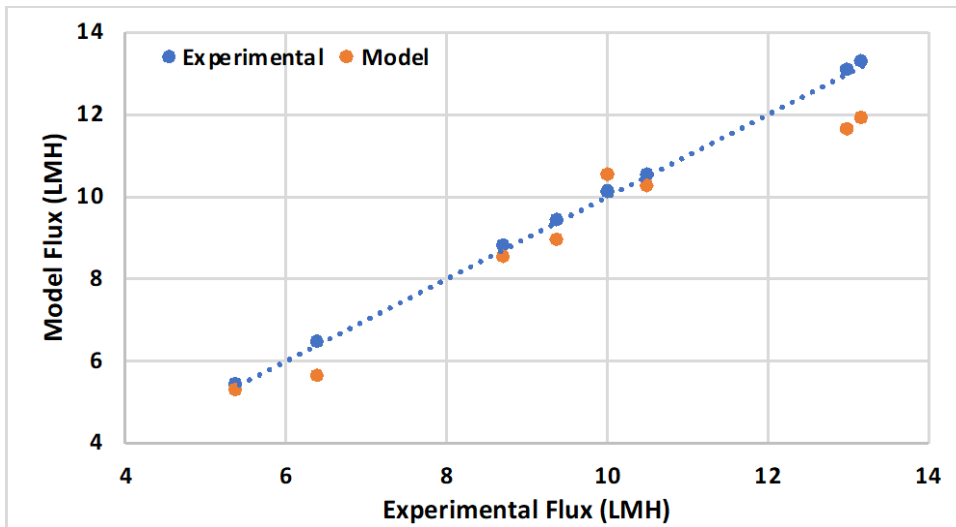
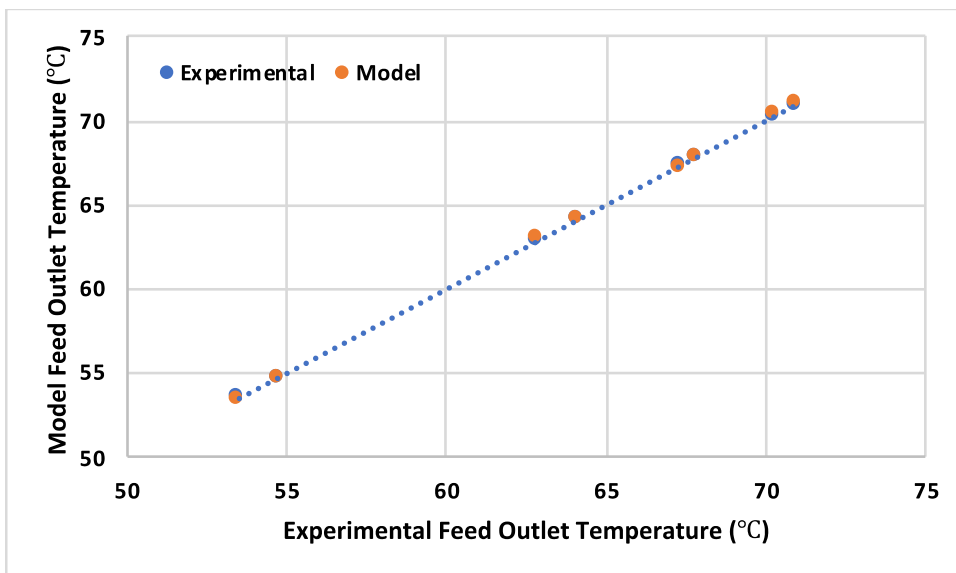Figure 16. Comparison of water flux between the model and the lab-scale experimental data

Figure 17. Comparison of feed outlet temperature between the model and the lab-scale experimental data
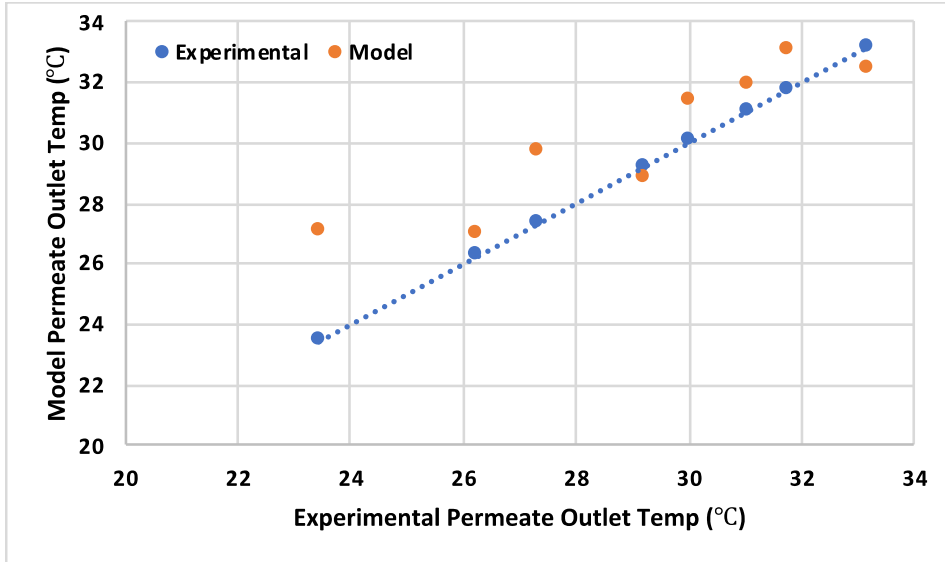
Figure 18. Comparison of permeate outlet temperature between the model and the lab-scale experimental data

Model error was quantified by employing a normalized mean absolute error (MAE) analysis. Normalization of error was required to obtain overall model error because of the wide range in the values being compared. Initial comparison of the model showed that there was a 6.71 percent error for flux, 0.18 percent error for feed outlet temperature, and 4.93 percent error for permeate outlet temperature. The goal of tuning was to minimize these errors as significantly as possible with lab-scale data so that error propagation can be reduced. The value for thermal conductivity was then adjusted within the defined range until the model matched experimental results. The thermal conductivity value that generated the most accurate model predictions was 0.175 W/m-K. The final tuning resulted in a 4.86 percent error in flux, a 0.25 percent error in feed outlet temperature, and a 4.10 percent error in permeate outlet temperature. The results can be seen in Figure 19, Figure 20, and Figure 12.
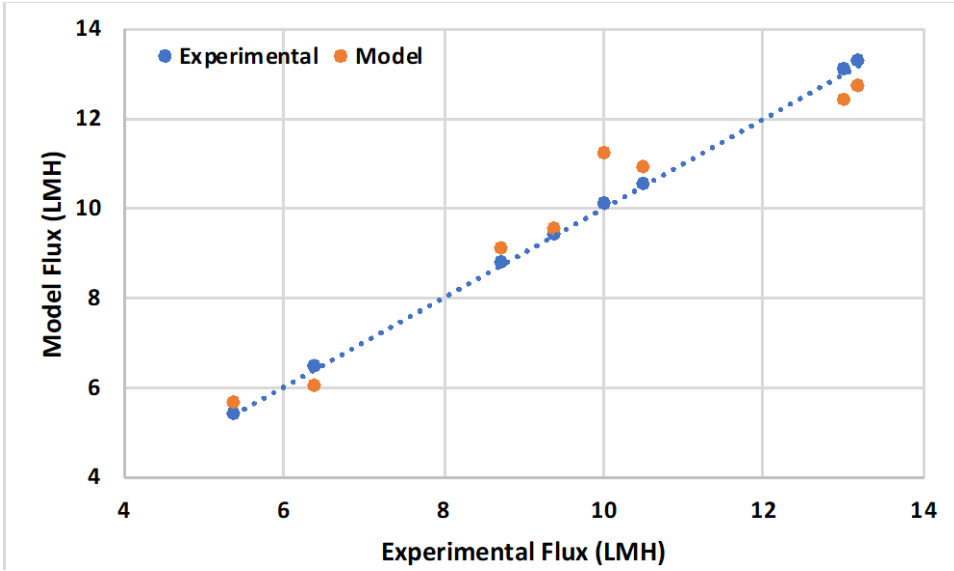
Figure 19. Comparison of water flux between the model and the lab-scale experimental data after tuning of membrane thermal conductivity
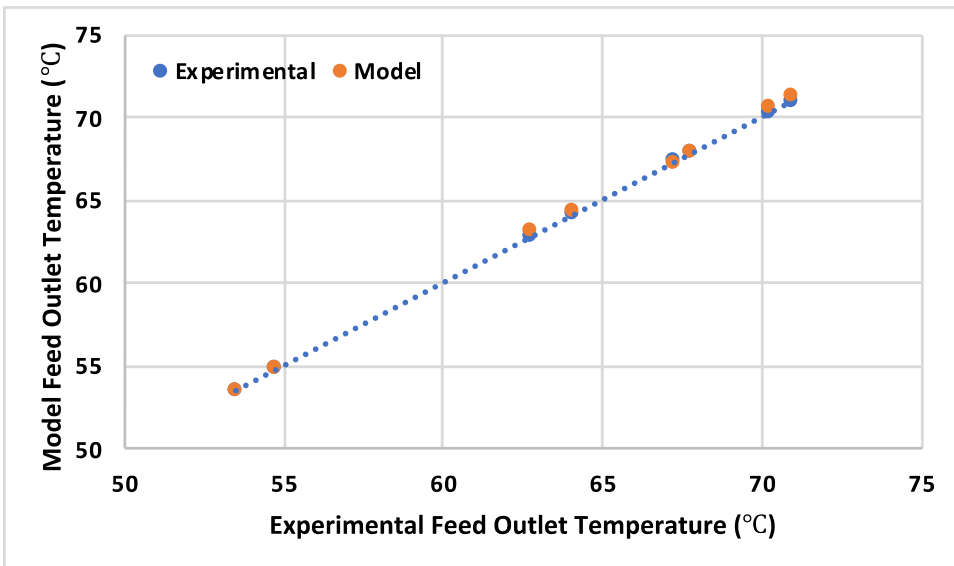
Figure 20. Comparison of feed outlet temperature between the model and the lab-scale experimental data after tuning of membrane thermal conductivity

Figure 21. Comparison of permeate outlet temperature between the model and the lab-scale experimental data after tuning of membrane thermal conductivity

The larger deviations in permeate outlet temperature were accepted because the error showed no bias to over/under-predicting the values; as a result, the deviations were attributed to random test errors. This concluded membrane characteristics tuning.

The model was then applied to data for the 25 percent and 50 percent packed modules. This was done to develop a regression for the effective surface area coefficient in relation to the module's packing density. The same process used for membrane characteristic tuning was implemented in tuning the coefficient. The baseline comparison used the thermal conductivity value previously tuned and assumed a 100 percent effective surface area. The comparison results for a 50 percent packed module show the necessity for implementation of such a coefficient in the model, as seen in Figure 22, Figure 23, and Figure 24.
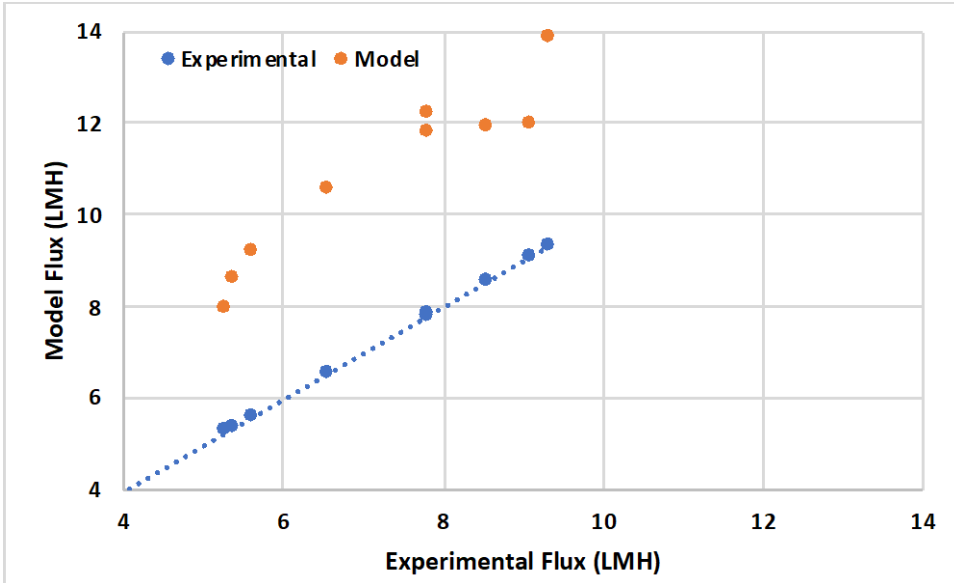
Figure 22. Comparison of water flux between the model and the lab-scale experimental data for 50 percent packing density
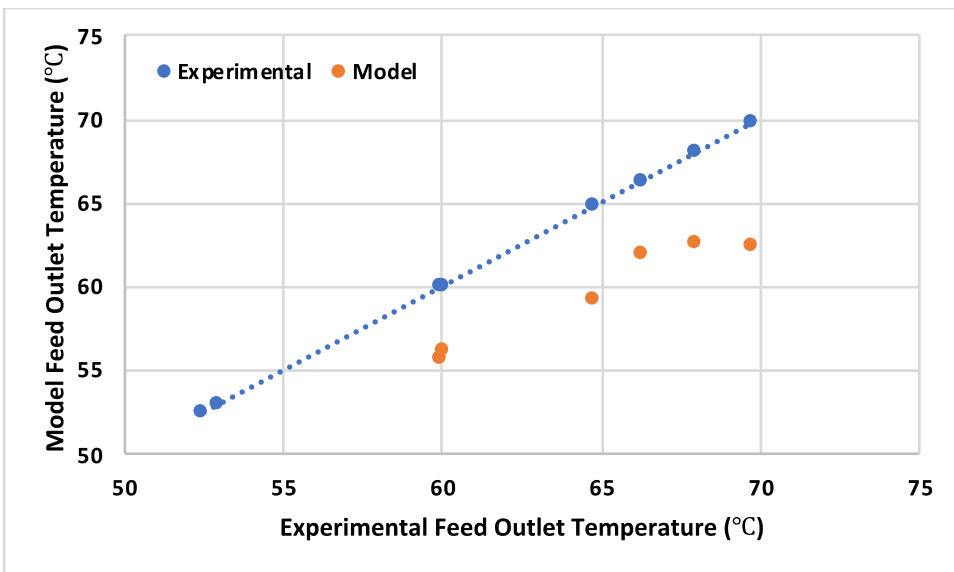
Figure 23. Comparison of feed outlet temperature between the model and the lab-scale experimental data for 50 percent packing density
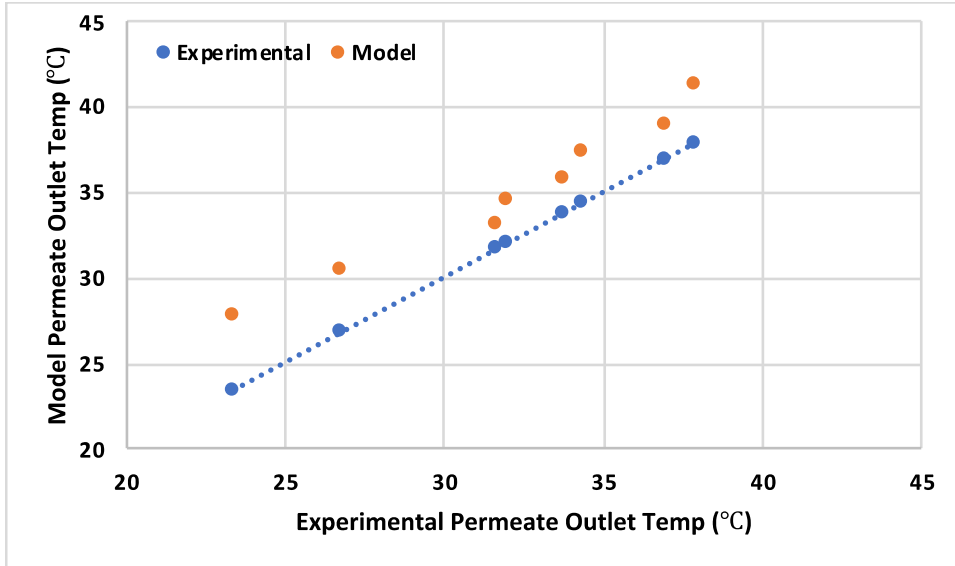
Figure 24. Comparison of permeate outlet temperature between the model and the lab-scale experimental data for 50 percent packing density

The initial comparisons resulted in a 51.57 percent error in flux, 7.50 percent error in feed outlet temperature, and 8.73 percent error in permeate outlet temperature. After tuning, the effective surface area was determined to be 65 percent for a 50 percent packed module. The implementation of the effective surface area coefficient into the model drastically improved model accuracy, as seen in Figure 25, Figure 26, and Figure 27.
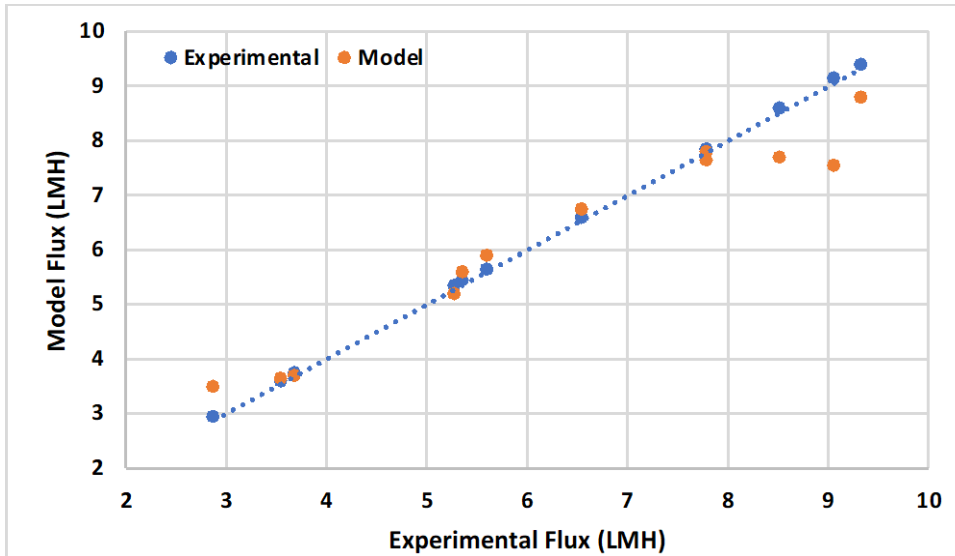
Figure 25. Comparison of water flux between the model and the lab-scale experimental data after tuning of effective surface area

Figure 26. Comparison of feed outlet temperature between the model and the lab-scale experimental data after tuning of effective surface area

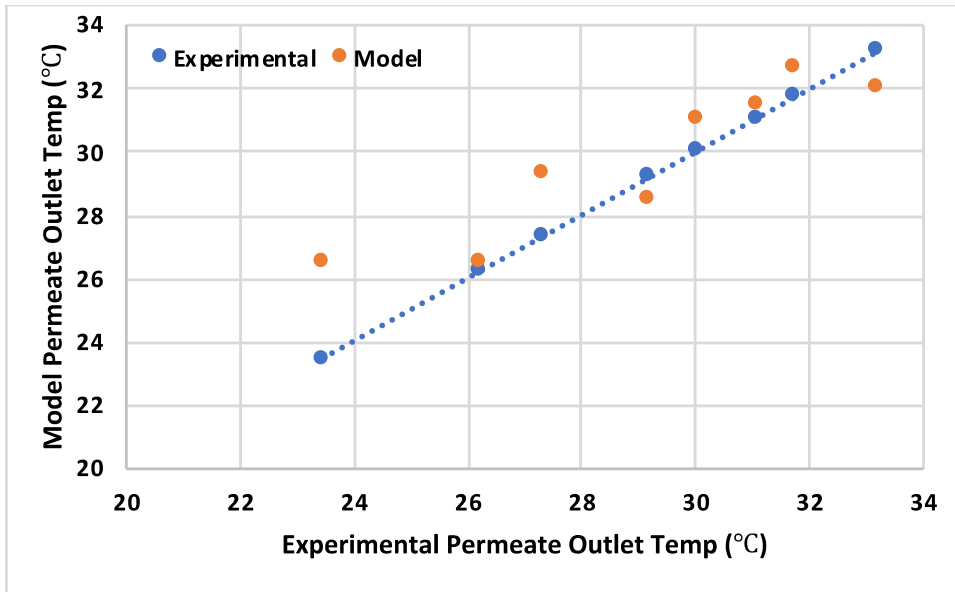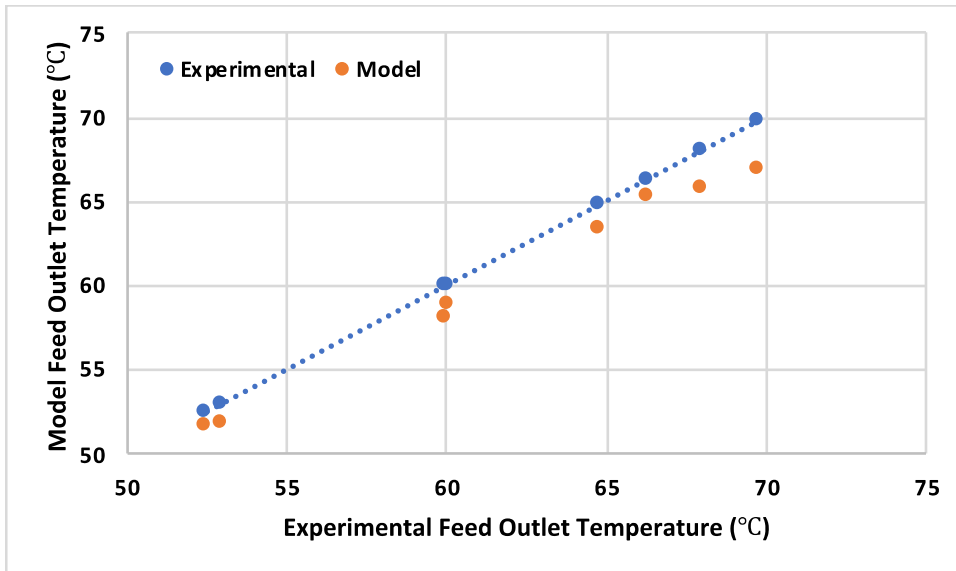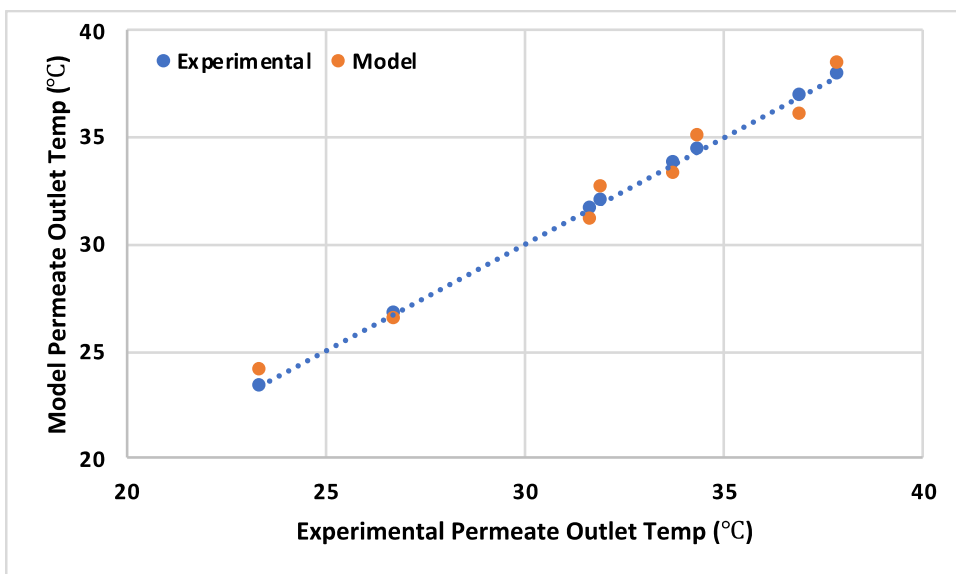**Figure 27. Comparison of permeate outlet temperature between the model and the lab-scale experimental data after tuning of effective surface area**

Table 6 provides a summary of lab-scale verification results and overall model error when applied to lab-scale modules of any packing density. This was done to provide a comprehensive analysis of model predictions across all module configurations.

Table 6. Summary of model tuning using lab-scale experimental data

Packing Density	Temp in (℃)		Flux (LMH)			Effective SA f	Flow Configuration	MAE%
	Hot	Cold	Model	Experimental	Error			
10%	65	22	9.25	9.4	1.55%	1	Feed on Shell	
25%	65	26	7.48	7.45	0.43%	0.75	Feed on Shell	4.01%
50%	64	31	6.00	5.29	13.43%	0.65	Feed on Shell	

Packing Density	Temp in (℃)		Hot Out (℃)			Effective SA f	Flow Configuration	MAE%
	Hot	Cold	Model	Experimental	Error			
10%	65	22	63.53	64	0.73%	1	Feed on Shell	
25%	65	26	61.88	62	0.20%	0.75	Feed on Shell	1.48%
50%	64	31	57.83	60	3.61%	0.65	Feed on Shell	

Packing Density	Temp in (℃)		Cold Out (℃)			Effective SA f	Flow Configuration	MAE%
	Hot	Cold	Model	Experimental	Error			
10%	65	22	30.36	31	2.08%	1	Feed on Shell	
25%	65	26	32.10	33	2.74%	0.75	Feed on Shell	2.17%
50%	64	31	35.60	35	1.72%	0.65	Feed on Shell	

A regression was developed to predict the effective surface area coefficient with respect to the module packing density of the pilot-scale modules and potentially large-scale modules. The regression is seen in Figure 27.

$$y = 0.5305x^{-0.27}$$
$$R^2 = 0.9876$$
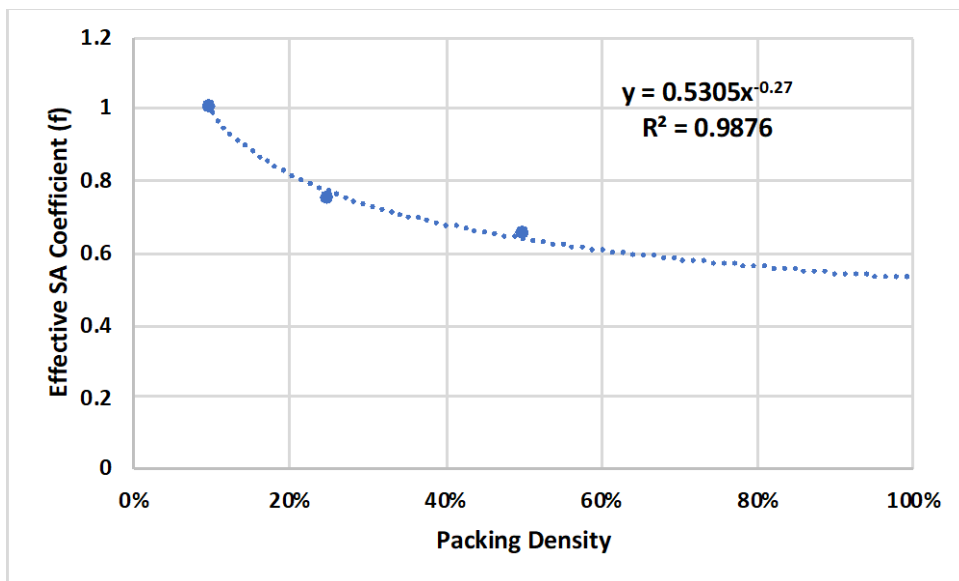
Figure 28. Correlation between effective surface area coefficient and module packing density

Using the regression developed for effective surface area coefficient, it was estimated that the effective surface area of a 70 percent packed module would be 58 percent. However, because the flow path was different between lab-scale modules and pilot modules – axial versus radial – the flow distribution inside the module was significantly different and resulted in deviation of the coefficient when comparing model predictions to pilot-scale experimental values. The true effective area is much lower than expected. This can be seen in Table 7, Table 8, and Table 9, which present summaries of all model verification results for lab and pilot-scale module comparisons.

Table 7. Performance model verification for module water flux

Module Description	Packing Density	Temp in (℃)		Flux (LMH)		Effective SA f	Flow Configuration
		Hot	Cold	Model	Experimental		
Lab Scale Modules	10%	65.00	22.00	9.25	9.40	1.00	Feed on Shell
	25%	65.00	26.00	7.48	7.45	0.75	Feed on Shell
	50%	64.00	31.00	6.00	5.29	0.65	Feed on Shell
Pilot Module 1	70%	81.43	25.37	2.65	3.07	0.23	Feed on Shell
	70%	82.19	30.06	2.70	2.91	0.23	Feed on Shell
	70%	82.25	34.91	2.66	2.83	0.23	Feed on Shell
	70%	83.29	40.46	2.66	2.77	0.23	Feed on Shell
Pilot Module 2	70%	53.62	33.43	0.96	0.73	0.21	Feed on Lumen
	70%	54.05	34.28	0.97	0.73	0.21	Feed on Lumen
	70%	55.50	35.80	1.02	0.73	0.21	Feed on Lumen
	70%	58.26	36.61	1.21	0.85	0.21	Feed on Lumen

Table 8. Performance model verification for module feed outlet temperature

Module Description	Packing Density	Temp in (℃)		Feed Out (℃)		Effective SA f	Flow Configuration
		Hot	Cold	Model	Experimental		
Lab Scale Modules	10%	65.00	22.00	63.53	64.00	1.00	Feed on Shell
	25%	65.00	26.00	61.88	62.00	0.75	Feed on Shell
	50%	64.00	31.00	57.83	60.00	0.65	Feed on Shell
Pilot Module 1	70%	81.43	25.37	49.82	50.27	0.23	Feed on Shell
	70%	82.19	30.06	52.52	52.64	0.23	Feed on Shell
	70%	82.25	34.91	55.09	55.35	0.23	Feed on Shell
	70%	83.29	40.46	58.45	58.66	0.23	Feed on Shell
Pilot Module 2	70%	53.62	33.43	48.74	49.52	0.21	Feed on Lumen
	70%	54.05	34.28	49.25	50.03	0.21	Feed on Lumen
	70%	55.50	35.80	50.68	51.44	0.21	Feed on Lumen
	70%	58.26	36.61	52.90	53.73	0.21	Feed on Lumen

Table 9. Performance model verification for module permeate outlet temperature

Module Description	Packing Density	Temp in (℃)		Permeate Out (℃)		Effective SA f	Flow Configuration
		Hot	Cold	Model	Experimental		
Lab Scale Modules	10%	65.00	22.00	30.36	31.00	1.00	Feed on Shell
	25%	65.00	26.00	32.10	33.00	0.75	Feed on Shell
	50%	64.00	31.00	35.60	35.00	0.65	Feed on Shell
Pilot Module 1	70%	81.43	25.37	41.42	41.12	0.23	Feed on Shell
	70%	82.19	30.06	45.12	44.47	0.23	Feed on Shell
	70%	82.25	34.91	48.71	48.20	0.23	Feed on Shell
	70%	83.29	40.46	53.10	52.41	0.23	Feed on Shell
Pilot Module 2	70%	53.62	33.43	39.85	39.28	0.21	Feed on Lumen
	70%	54.05	34.28	40.59	40.08	0.21	Feed on Lumen
	70%	55.50	35.80	42.13	41.61	0.21	Feed on Lumen
	70%	58.26	36.61	43.64	43.07	0.21	Feed on Lumen

The overall model errors associated with any of the applications were 7.95 percent error in flux, 1.14 percent error in feed outlet temperature, and 1.44 percent error in permeate outlet

temperature. The results provided sufficient evidence for model accuracy in heat and mass transfer predictions for lab and pilot-scale modules based on the 20 percent error goal. As a result, it was reasonable to use the model to predict mass and heat transfer parameters for large scale DCMD modules.

3.2.2.2. Pressure Model Verification

The models for predicting shell and lumen pressure could not be tuned because the model equations were based on experimental operational conditions (feed and permeate velocity), not physical properties associated with the module. Rather, the model was directly compared to supplemental experimental data – data not used to create the model – in order to verify its accuracy. The lumen pressure modeling equation integrates flux in its prediction; therefore, comparisons were made with tests where flux was observed and where flux was absent. The results for the lumen pressure predictions are shown in Table 10.

Table 10. Verification of the lumen pressure model

| Module | Flow Rate (gpm) | Lumen Pressure (psi) | | Description | MAE% |
		Model	Experimental		
Module 2	3	5.37	6.15	Flux	21.88
	4	8.14	11.10	No Flux	
	5.2	11.92	15.30	No Flux	

The large observed error is most likely associated with the fact the shell velocity/pressure is not integrated into the model equation. Since the fibers are not rigid tubes, shell pressure has a significant effect on the lumen pressure. However, more experimental data would be needed to develop a correlation for the impact of shell pressure on the lumen and account for this source of error.

The shell pressure model was developed solely from experimental data and was verified with data not used to construct the regression. Data for the shell pressure model accuracy are shown in Table 11.

Table 11. Verification of the shell pressure model

| Module | Flow Rate (gpm) | Shell Pressure (psi) | | MAE% |
		Model	Experimental	
Module 2	1.9	12.40	10.69	6
	2.6	18.86	20.10	
	2.7	18.60	19.50	
	2.8	18.76	18.70	

The shell pressure model was determined be much more accurate than the lumen pressure model. This may be attributed to the model equation integrating the effects from the lumen operating pressure. The results from the two pressure model comparisons verified their applicability in predicting module operation and could, in turn, be used to estimate performance of large-scale DCMD modules.

3.2.3. Overall Performance Model for use in DCMD System Design

Once verified, the model was adjusted to make it more user friendly and to simplify the design process. Additionally, an Excel add-in for the model was developed so that potential users would not need MATLAB to design a DCMD system.

3.2.3.1. User Inputs and Defaults

Two tiers of inputs from the user were required for design purposes. Tier 1 information represented the minimum amount of information that the user had to supply to the model. This included information about the DCMD module geometry and operational conditions of the system. Tier 2 information represented supplemental information about the membrane characteristics that the user could provide to obtain a more accurate performance prediction. If the information was not available to the user, default values would be used for computations; the defaults were based on characteristics of PTFE hollow fibers used in Markel Corporation DCMD modules. All other information needed for performance predictions are either defined or derived within the model code and cannot be altered by the user. The list of Tier 1 and 2 inputs is shown in Figure 29.

Figure 29. User input interface in Excel of the full-scale DCMD performance model

3.2.3.2. Excel Add-In and User Interface

MATLAB's Library Compiler application was used to generate an Excel add-in that could be implemented into a spreadsheet in order to perform the model calculations without the need for MATLAB on the computer; rather, the add-in uses an online run-time to execute performance calculations and output the results into the selected spreadsheet range. A flow diagram for general functionality of the add-is provided in Figure 30. Implementation of the add-in into a spreadsheet is shown in Figure 29.
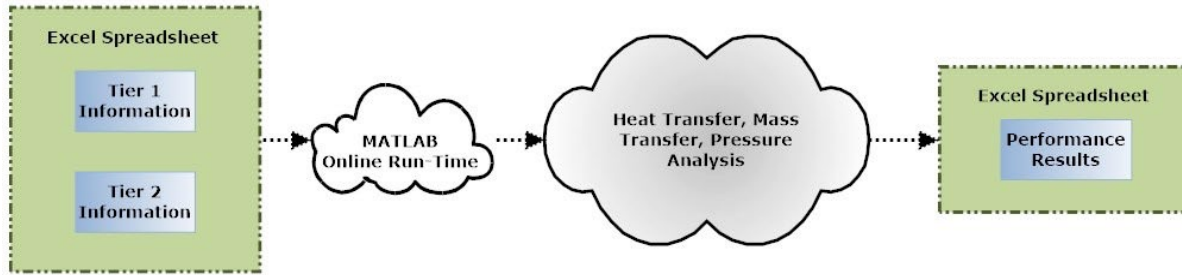
Figure 30. Functionality of the MATLAB-based Excel add-in

3.2.3.3. Model Constraints

The current version of the model has several constraints that need to be taken into consideration before use in DCMD system design. The model is designed for co-current feed and permeate flow through the module, with the feed going through the lumen and permeate on the shell. The well flow rate should be greater than the feed flow rate or the model will error and give incorrect water production estimates. The model is tuned for DCMD modules that utilize PTFE HFMs; discrepancies may occur for other HFM materials such as PVDF and PP. A regression was developed to determine the number of fibers (for use in calculating SA) based on the diameter of the module; however, this regression is only applicable for fibers with an outer diameter of 0.0018 m. Inaccurate predictions may occur if the fiber outer diameter is significantly different than 0.0018 m. Modeling divergence is often an indicator that an error has occurred in heat transfer calculations; values for membrane characteristics should be checked. Random values should not be entered for membrane properties; only measured values or those given by the membrane manufacturer should be used. Since properties are theoretically dependent on one another (i.e., porosity and thermal conductivity), they should not be adjusted independently; wall thickness is the only value that can be manipulated independently for performance predictions.

3.2.4. Design Guidelines Based on Performance Modeling

The construction of a guideline that outlines a standard approach in designing large-scale DCMD systems is important to provide to users, as it ensures that the recommended operational conditions and system construction requirements are as accurate as possible. Additionally, it provides users with a basic understanding of how the model can be used in large-scale system design.

For input parameters that can be adjusted or chosen by the user, it is important to provide supplemental information that can be used to determine optimal performance values. For example, there are various commercially available module geometries for DCMD; performance charts for each module configuration would help the user determine which module to use for large-scale system design. Similarly, charts should provide optimal flow rates that should be pumped through the module to achieve the desired water production performance.

3.2.5. Implications for Large-Scale DCMD Applications

Once the performance model accuracy was verified using pilot-scale data, it was used to predict the performance of larger modules that would be used in industrial applications. The model was used to generate data that would express the impacts of module geometry, membrane property, flow velocities, and flow configuration (feed on shell or lumen) on overall flux and module design efficiency. The results of such impact studies would establish merit for researching improvements in module design and membrane properties. The analysis was conducted for a 14-by 40-inch DCMD module that utilized PTFE HFMs. Effective area coefficients of 0.21 and 0.9 were chosen for comparison; 0.21 is the current effective surface area coefficient determined for 70 percent packed pilot-scale modules, while 0.9 is a theoretical value for the coefficient in the case that future designs are improved. Maximum flow rates were determined based on their associated system pressures reaching the maximum allowed module pressure; additionally, since the pressures were calculated using feed and permeate velocities, using the maximum pressures ensured that the velocities were equivalent for proper comparison. The membrane wall thickness and thermal conductivity analyses were performed with an effective surface area coefficient of 0.9. The design efficiencies of the module configurations were determined based on Equation 36. Summaries of the analysis are shown in Table 12 and Table 13.

$$\text{Design Efficiency} = \frac{\text{Distance from inlet where flux is 50\% of average flux}}{\text{Total length of module}} \tag{36}$$

Table 12. Analysis of design efficiency for large-scale DCMD modules with feed on the lumen

	Feed on Lumen							
	Feed Flow (gpm)	Permeate Flow (gpm)	Average Flux (LMH)	Effective Module Length (cm)	Length of Module (cm)	Design Efficiency	Feed Temp at Equivalence (℃)	Permeate Temp at Equivalence (℃)
Effective SA 0.21	1	1	0.03	6	102	6%	62.5	62.5
	1	30	0.05	8	102	8%	46.2	46.1
	350	1	0.08	8	102	8%	79.9	79.8
	350	30	2.11	66	102	65%	77.5	73.1
Effective SA 0.9	10	10	0.34	12	102	12%	62.7	62.4
	10	120	0.49	15	102	15%	48.5	47.6
	350	10	0.82	15	102	15%	79	78.6
	350	120	6.60	56	102	55%	72	68.2
Membrane Wall: 50% Thickness	10	10	0.30	9	102	9%	62.7	62.4
	10	120	0.43	11	102	11%	48.1	47.7
	350	10	0.73	11	102	11%	79	78.6
	350	120	5.97	42	102	41%	71.7	69.2
Thermal Cond. 0.04 W/m-K	350	120	10.71	70	102	69%	72.3	67.2

Table 13. Analysis of design efficiency for large-scale DCMD modules with feed on the shell

	Feed Flow (gpm)	Permeate Flow (gpm)	Average Flux (LMH)	Effective Module Length (cm)	Length of Module (cm)	Design Efficiency	Feed Temp at Equivalence (℃)	Permeate Temp at Equivalence (℃)
	Feed on Shell							
Effective SA 0.21	1	1	0.03	3	102	3%	62.5	62.4
	30	1	0.06	6	102	6%	78.9	78.8
	1	350	0.04	6	102	6%	45.2	45.1
	30	350	1.17	59	102	58%	52.7	47.3
Effective SA 0.9	10	10	0.26	9	102	9%	62.6	62.3
	120	10	0.59	12	102	12%	77.3	77.0
	10	350	0.39	13	102	13%	46.8	45.9
	120	350	4.19	49	102	48%	57.0	52.8
Membrane Wall: 50% Thickness	10	10	0.27	8	102	8%	62.6	62.4
	120	10	0.60	10	102	10%	77.3	77.0
	10	350	0.39	10	102	10%	46.6	46.0
	120	350	4.21	39	102	38%	56.2	53.2
Thermal Cond. 0.04 W/m-K	120	350	7.76	63	102	62%	58.7	52.2

The results of the analysis show that increasing the effective area coefficient has a significant effect on overall performance and that further research into improving flow distribution to obtain a value of 0.9 should be conducted to maximize water production. Furthermore, changing the physical property of the membrane to lower the thermal conductivity would have the greatest impact on improving module performance; reduced membrane conductivity produced the highest flux and drastically enhanced the design efficiency. This was most likely due to the fact that decreasing the thermal conductivity reduced the temperature polarization observed in the boundary layers. Conversely, reducing the membrane wall thickness inhibits performance improvements because temperature polarization becomes more significant in the boundary layers.

3.3. Techno-Economic Model

3.3.1. Model Design and Implementation

The techno-economic model was designed to be as user friendly as possible and require the least amount of input values to come up with an appraisal level cost of a DCMD system. One would simply need basic operational conditions, module geometry, and desired production rates; other values such as membrane characteristics would be set at default values that the user could change if the information is known. The required information includes the desired product flow rate, feed inlet temperature, permeate inlet temperature, ambient air temperature, and then the feed and permeate streams' flow rates. These are input into the "user inputs" tab of the model; then, using the DCMD add-in, the performance of the DCMD modules can be determined. The resulting information is then used for the sizing of all of the units to deliver the desired product

flow rate. The resulting costs for the units are then outputted in the "report" tab. The user can consult these costs and then return to the user inputs to modify the flow rates for the DCMD modules.

In estimating the costs of these unit processes, previous cost equations for the acid pretreatment, microfiltration, pH readjustment, and reinjection wells were utilized. However, the cost equations do not exist yet for DCMD since the technology has not been implemented on a large scale, so they were estimated using membrane cost per square meter, as seen in the following section. Air coolers had also never been incorporated into a desalination plant's appraisal, so the costs of air coolers were estimated using the chemical engineering cost estimation program CAPCOST.

3.3.1.1. DCMD Modules

The design process for the DCMD modules can be seen in Figure 31, which depicts all of the input parameters and what they affect for the overall DCMD system. The design of the DCMD modules for the techno-economic analysis used a 14-inch diameter by 40-inch length module, a feed water temperature of 80°C, a desired inlet permeate temperature of 45°C, and the desired production rate of 160 gpm.
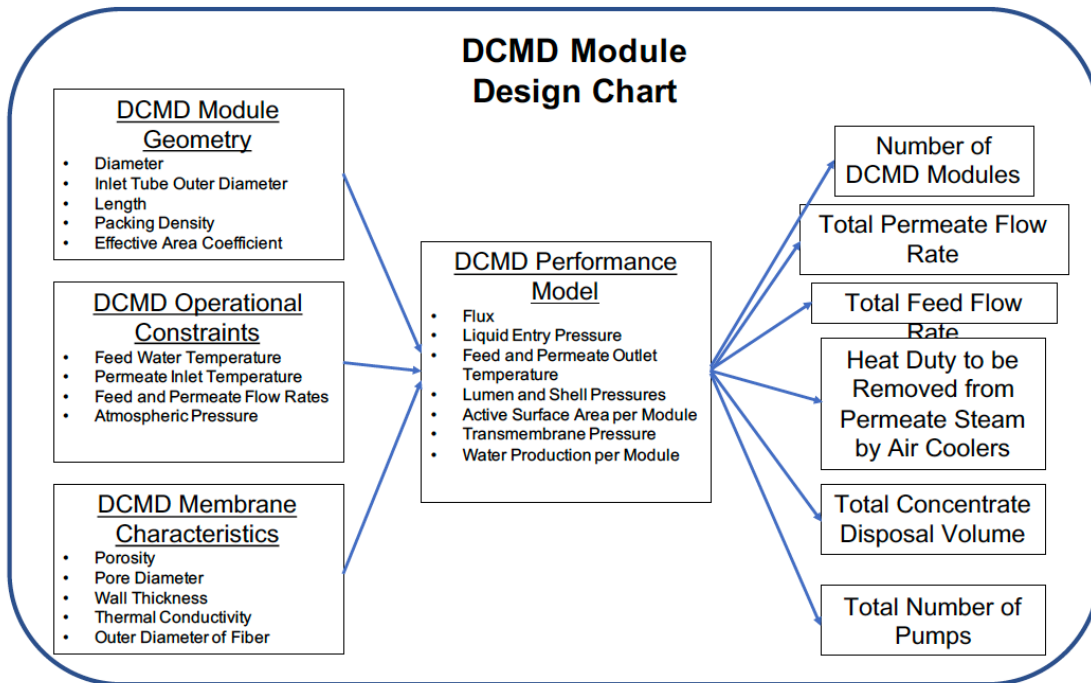

Figure 31. DCMD module design process in the techno-economic model

Since there are no known relations developed for the cost of DCMD modules, a curve was constructed based on the prices of various size DCMD modules from U.S. manufacturers as shown in Figure 32. This was to provide a cost per square meter of membrane based on available module diameters. This value can then be used to determine the cost of the module based on the total surface area needed to obtain the desired production rate.
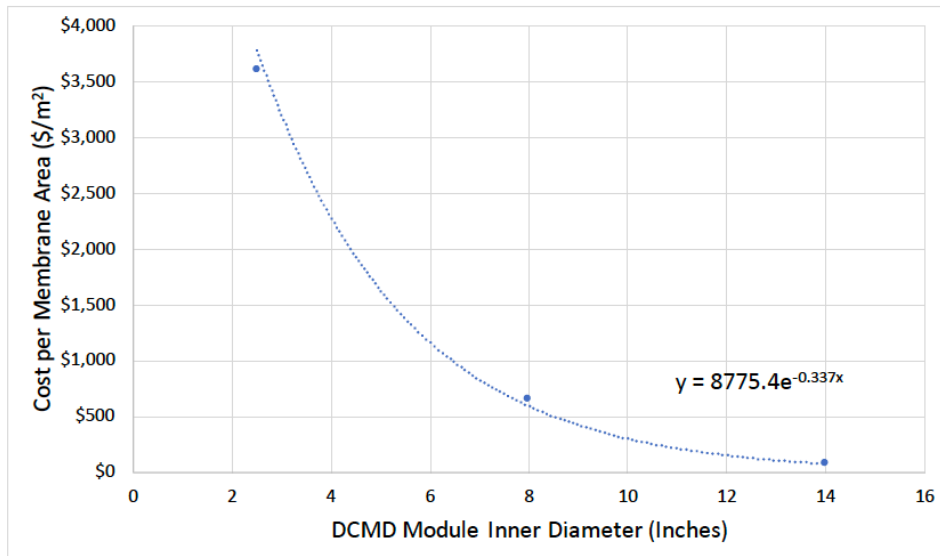
The plot shows a scatter of data points with a dotted trend line. The equation displayed on the chart is:

$$y = 8775.4e^{-0.337x}$$

Figure 32. Cost of DCMD modules ($/m² of membrane area) based on module inner diameter

3.3.1.2. Filtration

The microfiltration unit for the DCMD system was equipped with a regenerative and cartridge-based sizing analysis, which uses the set feed flow rate from the DCMD modules to determine the necessary total feed flow rate. The regenerative microfiltration unit applies user inputs for membrane module characteristics, operational inputs, and operating conditions. These parameters determine the amount of membrane area required and the actual delivered feed flow rate, which are used to calculate the capital costs associated with the unit as well as its feed and backwash pump. The cartridge microfiltration unit employs a design flux, transmembrane pressure, and membrane area per module, which are all set by the user. These then determine the number of modules and the overall cost, which are calculated using CAPCOST.

3.3.1.3. pH Adjustment

pH adjustment through acid injection is a necessary as a pretreatment method, as the geothermal brackish water typically presents with a high membrane fouling potential that needs to be addressed. Additionally, the pH needs to be readjusted post processing near the original pH to prevent degradation of the aquifer when it's reinjected. Acid pretreatment and pH readjustment were calculated using the water chemistry of the feed water with a primary focus on the carbonate-based alkalinity to determine the necessary dosing rates. These dosing rates were then used to estimate the total costs for each unit by using the capital and O&M cost equations.

3.3.1.4. Air Cooled Heat Exchangers

The air-cooled HEs are essential units for DCMD desalination systems, as they provide the necessary cooling of the permeate recycle water to maintain the vapor pressure gradient to drive the flux. Proper sizing calculations based on atmospheric conditions of the site are exceedingly pertinent to maintaining DCMD systems in various locations that these DCMD systems may be

utilized. The design and sizing of air-cooled HEs involves several assumptions as outlined below.

- Outer tube diameter: 1 inch
- Fin height: 0.625 inch
- Number of fins per inch of tube: 10
- Tube length: 32 feet
- Tube pitch: 2.5 inches
- Number of passes: 1 pass

It is also important to acknowledge that ambient air temperature plays a significant role in the applicability of the unit because there is an associated economical approach temperature associated with the cooling factor. This lower economical approach temperature sets a lower limit for an air cooler to cool a liquid and is generally 10-12°C higher than ambient temperature; in other words, if ambient temperature is 20°C, the HE would only be able to cool the liquid between 30-32°C without significant capital expenditure. The air cooler must be sized to the average air temperature of the summer months to maintain the desired water production. The air coolers can be sized and then cost estimated using CAPCOST. The number of transfer units (NTU) method of sizing was used to determine the best approximated values for the air coolers based on the incoming permeate water temperature, air temperature, desired outlet temperature, and the estimated heat transfer coefficient. The flow diagram in Figure 33 includes the general design procedure for the air coolers.
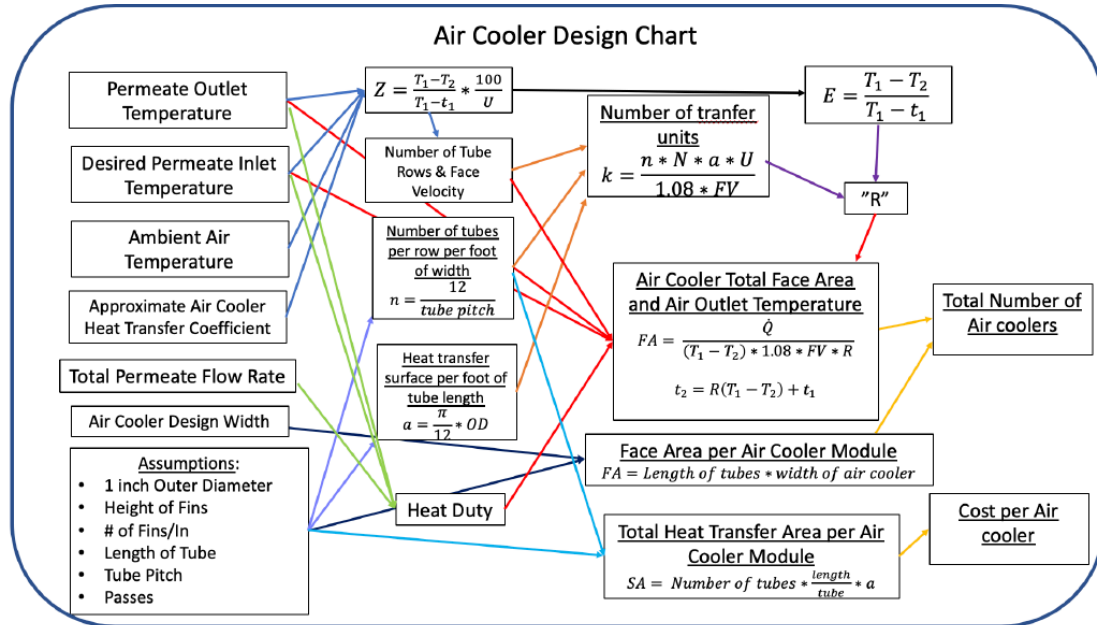

Figure 33. Air cooler design process for full-scale DCMD systems

3.3.1.5. Concentrate Disposal

Disposal of the concentrate water has two possible routes, which include a reinjection well or evaporation ponds. These disposal techniques are chosen by the user considering land

availability and the ability to drill reinjection water wells in that region. The cost analysis for the evaporation ponds is determined using the evaporation rate of the location, the liner thickness, purchase cost of the land, and land clearing costs. The reinjection well takes into consideration the depth of the well, and diameter of the pipe. For the cost analysis of the large-scale DCMD system, the depth of the well was considered to be 1,000 feet and the diameter to be 5 inches.

3.3.2. Optimization Analysis

The objective of the techno-economic analysis was to determine the viability of a DCMD system meeting typical production demands and competing with RO. Conditions and production requirements at Masson Farms were used to perform such analysis. Based on the current capacity of the RO system at the greenhouse, a production capacity of 230,000 gallons per day was required. The maximum available temperature from the geothermal well was determined to be 80°C. Ambient temperature at the greenhouse location could reach 40°C during the summer months; sizing should be based on ambient temperature during the summer months to ensure required production is met since the reduction of permeate cooling inhibits production potential.

Additional assumptions and constraints were made to perform the analysis, as listed below.

- Produced water flow rate of 160 gpm
- Feed water temperature of 80°C and composition remains constant
- Permeate inlet temperature 45°C
- Ambient air temperature 40°C
- Disposal of brine using an injection well
- DCMD module geometries were constant
- Geothermal well drilling and maintenance were ignored for cost estimation

Three scenarios were developed for cost estimation:

- Performance is equivalent to currently available DCMD modules (active surface area is 21 percent)
- Performance increased through potential DCMD module design improvements (active surface area is 65 percent)
- Maximum theoretical performance is achieved through design improvements (active surface area is 90 percent)

By conducting the analysis for all three scenarios, the viability for DCMD can be definitively established.

3.3.2.1. Optimization of Module Flux

The purpose of optimizing flux is to determine the conditions that are the most conducive for the maximum amount of water production per DCMD module to reduce the total number of modules. For the purpose of this techno-economic model, the 14-inch diameter by 40-inch length DCMD modules were used because of their high membrane area. It has been determined in previous lab-scale experiments that DCMD showed increased water production when the

permeate and feed streams were at the highest flow rates achievable. However, these high flow rates are limited by the current design of the DCMD modules, which prevents adequate flow distribution. This limited flow distribution causes a reduction in the active surface area within the module, resulting in diminished overall water production. Under the current design of these DCMD modules, upper limits for the feed and permeate streams per module were determined to be 300 gpm and 35 gpm, respectively. These flow rates were determined by monitoring the reported transmembrane pressure, which cannot exceed the liquid entry pressure set by the feed temperature. This liquid entry pressure is a function of the feed temperature; as the feed temperature increases, this liquid entry pressure will decrease due to the increased potential for pore wetting. Under the maximum flow regime achievable, the flux generated was 2.3 L/m²-h, which can be seen in Figure 34. The resultant flux is much lower than that observed in lab-scale experiments; this sheds light on the concept that the limiting factor for large-scale DCMD modules is their flow distribution design.
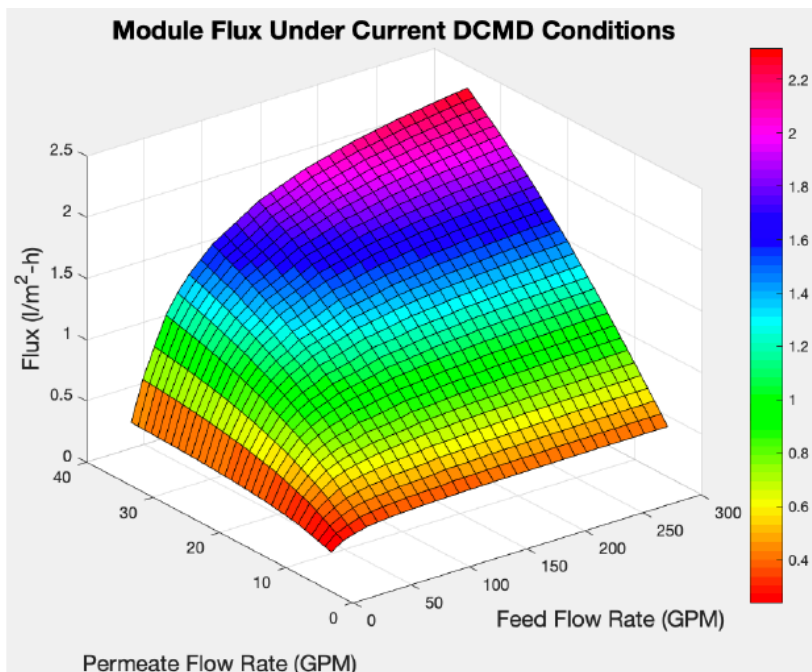

Figure 34. Module flux under the current DCMD conditions

With the information collected above for the current DCMD modules, the predicted water flux for the enhanced DCMD and theoretically superior DCMD modules were also explored. With the improved active surface area coefficient of 0.65 for the enhanced DCMD modules, the limits for the permeate and feed flow rates were raised significantly, which provided a much larger range of potential flow rates for optimization. The reason for this is that as the active surface area increases, there is an increase in volume within the module for water to flow, which permits increased flow rates.

In Figure 35, these increased ranges for the feed and permeate streams can be seen to stretch from 0-300 gpm and 0-150 gpm, respectively. The maximum flux that was achieved at the highest flow regime was recorded to be 6.72 L/m²-h, and the lowest flux can be observed as

0.85 L/m²-h. This lower limit shows that with the enhanced flow distribution and under the least ideal conditions, these modules are comparative to the current DCMD modules.
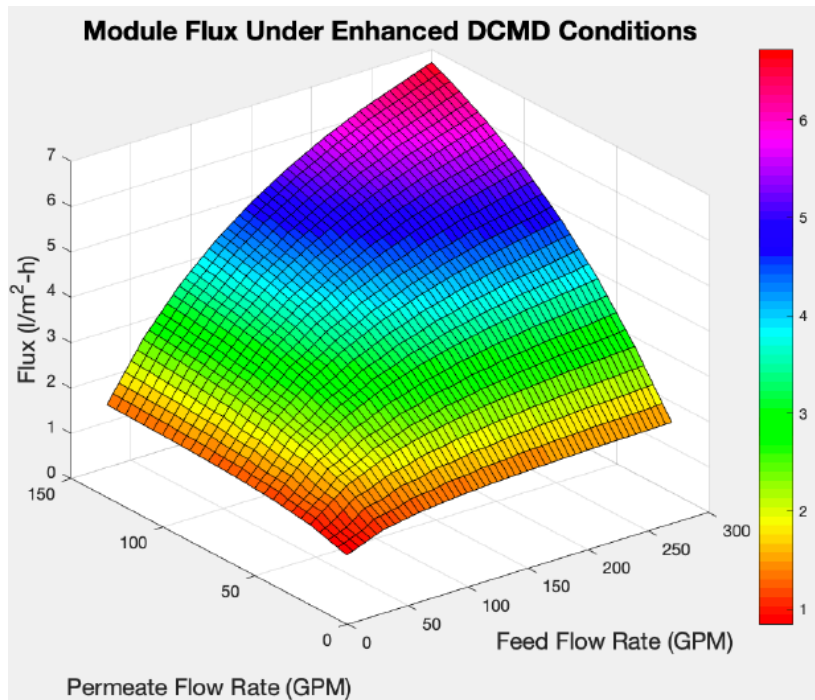

Figure 35. Module flux under the enhanced DCMD conditions

The flow rates for the theoretically superior modules, with an active surface area coefficient of 0.9, were analyzed and the permeate stream was capable of being slightly increased from the ranges of the enhanced module. However, when this higher flow regime was tested, the change in the maximum flux was insignificant in comparison to the enhanced DCMD module. As a result, the flow rate ranges that were found for the enhanced DCMD module were held constant for the theoretical module. The maximum flow regime of 300 gpm and 150 gpm for the feed and permeate streams, respectively, was able to produce a flux of 7.1 L/m²-h; the lowest flux observed was 0.84 L/m²-h as shown in Figure 36.
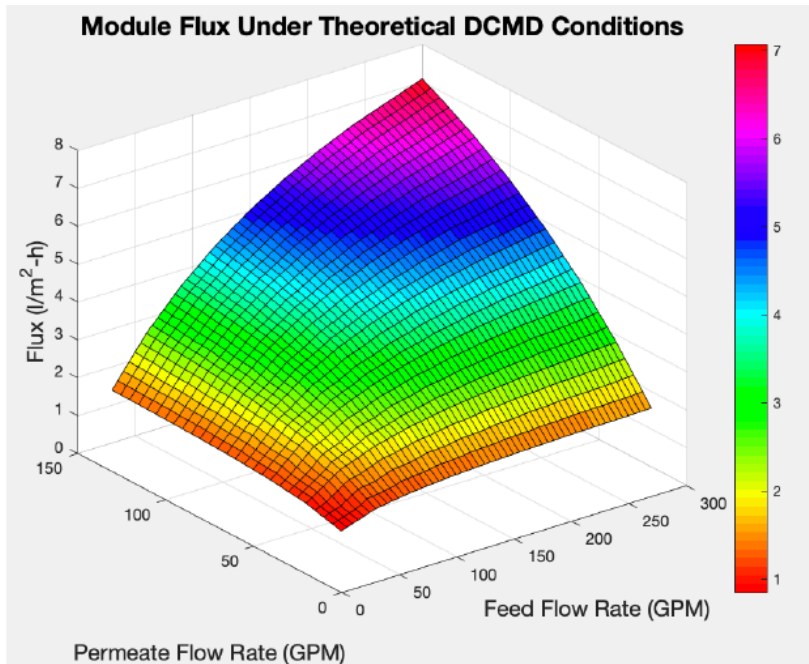
Figure 36. Module flux under the theoretical DCMD conditions

Using the maximum flux and the active surface area per module (m²/module), the water production per module can be calculated and the DCMD module designs can be compared. These data are shown in Table 14.

Table 14. Summary of module output based on flux optimization

DCMD Module Design	Flux (L/m²-h)	Available Membrane Area (m²/module)	Water Production per Module (L/h)
Current	2.3	18.8	43.6
Enhanced	6.7	58.3	391.5
Theoretical	7.1	80.7	571

It can be noticed that the water production per DCMD module increases significantly with an increased active surface area, even though there is an insignificant increase in flux from the 65 percent to 90 percent modules. The theoretical module design has the capability to produce 150 percent and 1,300 percent more water per module in comparison to the enhanced and current designs, respectively. In terms of optimization for the flux of the DCMD modules using the available membrane technology, a path towards making DCMD more efficient is to improve the flow distribution.

3.3.2.2. Optimization of Overall Cost

In order to produce an appropriate appraisal level cost estimation for the large-scale DCMD system, it is important to take all of the major components into consideration. Doing this incorporates all of potential contributors to the total cost when deciding the processing flow rates for designing the system, as each of these systems provide an area of optimization. However, optimizing for the lowest total cost of the facility neglects the total optimization of the

flux of the DCMD modules, this seems counter-intuitive considering maximum flux means increased water production. But the opposite is true because the conditions that are conducive to high fluxes do not reflect the optimal conditions for the other components in the system, specifically the air coolers.

The completed total cost analysis of the DCMD system using the current module design can be seen in Figure 37, with the lowest total cost for all components estimated to be $154.1 million and the feed and permeate stream flow rates set at 80 gpm and 30 gpm, respectively. These flow rates produced a flux of 1.6 L/m²-h, which is substantially less than the maximum flux the module can produce. The units that contributed the most to the total cost were the air coolers and DCMD modules and their respective equipment, which were estimated at $97.5 million, 63.3 percent of the total cost. The cost of the DCMD and HE equipment can be seen in Figure 38 for the current DCMD module design. It can be seen that the HE and DCMD units had a lower capital cost. However, the flow rates that create this cost do not provide the ideal conditions for the overall lowest cost.
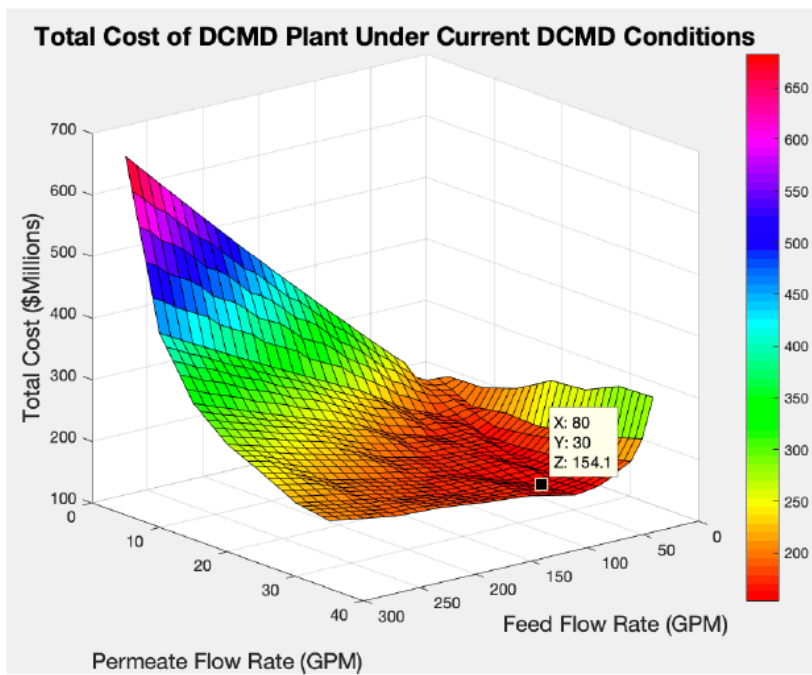

Figure 37. Total capital cost of a DCMD plant under the current DCMD conditions
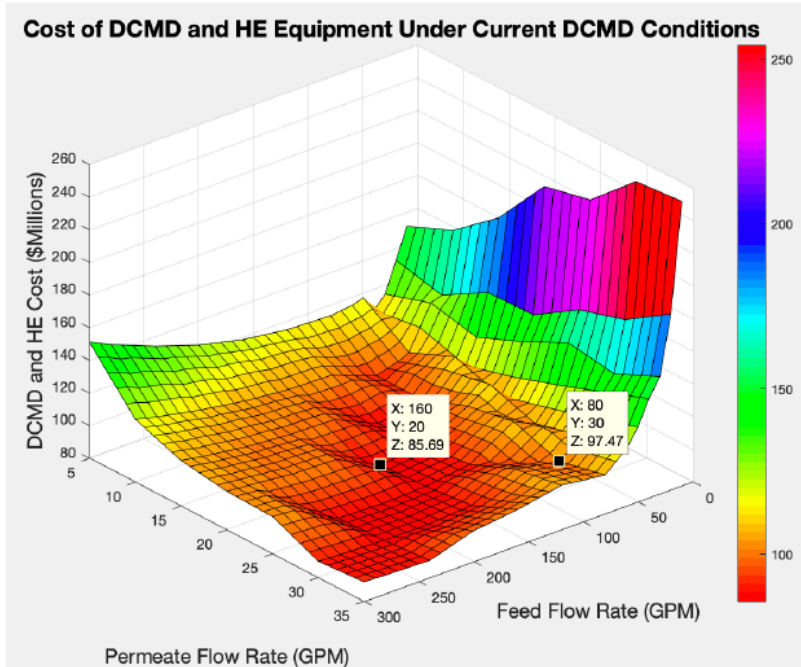
Figure 38. Capital cost of the DCMD and HE equipment under the current DCMD conditions

In the analysis of the total cost for the enhanced DCMD module in Figure 39 with a 65 percent active surface area coefficient, the lowest total cost was determined to be $54.3 million. The flow rates for the feed and permeate streams were set at 90 gpm and 40 gpm, respectively, and the flux of the modules was calculated to be 2 L/m²-h. The cost of the DCMD and HE equipment can be seen in Figure 40, which was estimated to be $31.5 million. These units accounted for 58 percent of the total cost for the DCMD system.
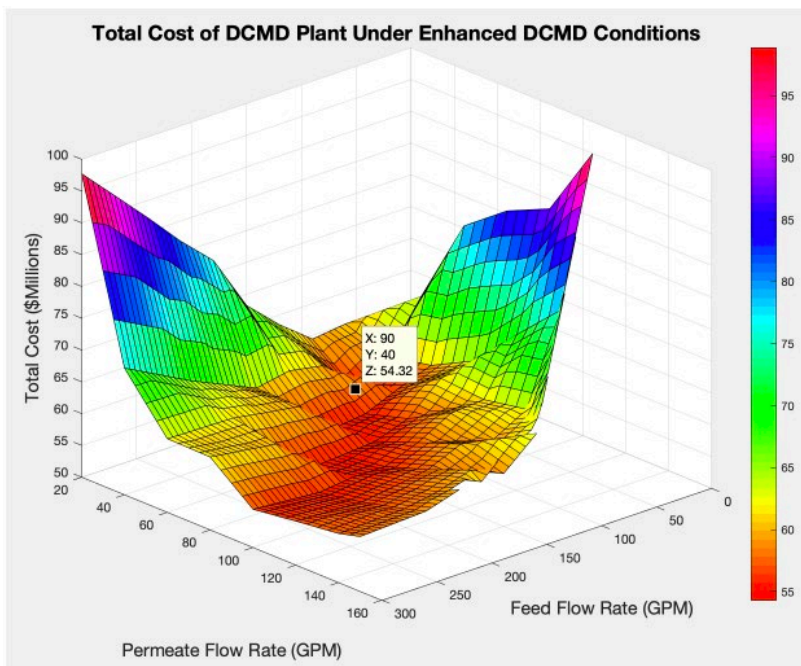

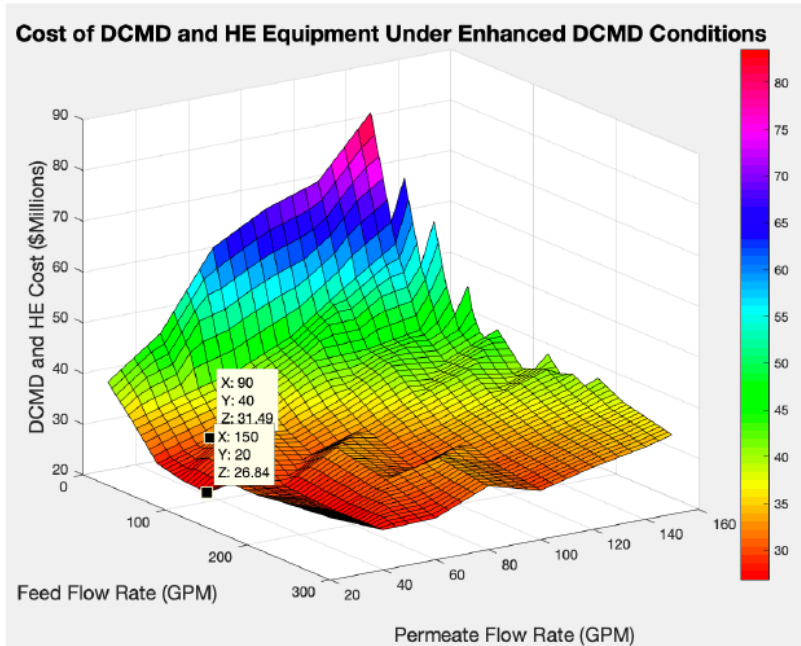**Figure 39. Total capital cost of a DCMD plant under the enhanced DCMD conditions**

Figure 40. Capital cost of the DCMD and HE equipment under the enhanced DCMD conditions

The cost analysis for the theoretical module design can be seen in Figure 41 yielded an estimated total cost of $41.1 million, with feed and permeate flow rates set at 210 gpm and 80 gpm, respectively. The DCMD modules at the set flow rates for the feed and permeate produced a flux of 4.31 L/m^2-h. The cost of the DCMD and HE equipment in Figure 42, was found to be $21.4 million, which contributed 52 percent of the overall cost.
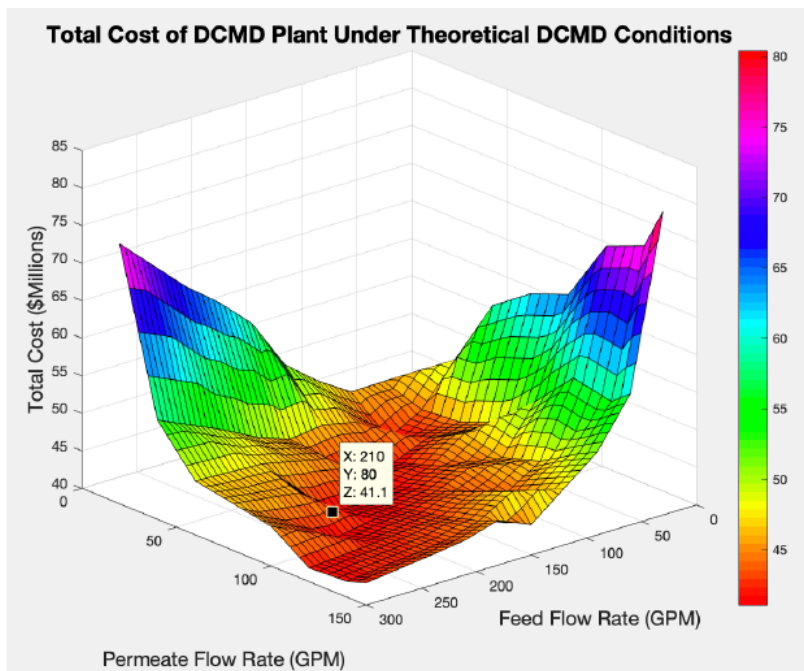

Figure 41. Total capital cost of a DCMD plant under the theoretical DCMD conditions
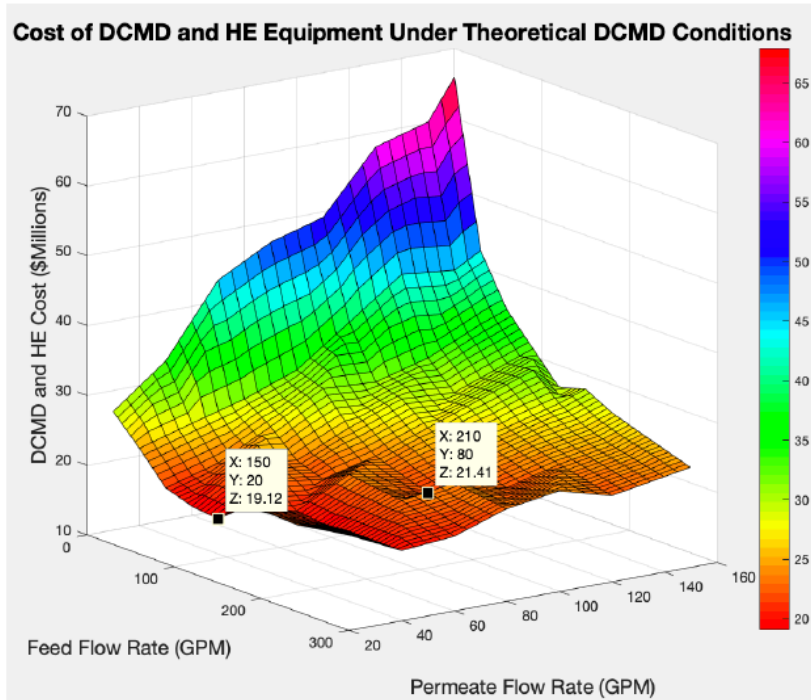
Figure 42. Capital cost of the DCMD and HE equipment under the theoretical DCMD conditions

Table 15 presents the minimal capital cost of the DCMD plant and the associated system specifications under each DCMD module design.

Table 15. Capital cost of the DCMD plant and the associated specifications

Plant specifications	DCMD Module Design		
	Current	Enhanced	Theoretical
Minimal capital cost (million $)	154.1	54.3	41.1
Number of DCMD modules	1241	307	104
Number of HE modules	124	41	28
DCMD & HE capital cost ($ million)	97.5	31.5	21.4
Membrane area (m^2)	18.1	58.3	80.8
Flux (L/m^2-h)	1.6	2	4.3
Water production (L/h)	29.2	117	347

The effective membrane area has a significant impact on the total cost of the DCMD system. This improvement allows for much more flow per module to produce increased fluxes despite the sub-optimal flow conditions. The result is greater water production per module, which cuts down the number of DCMD and HE modules. The reason these two units are the main focus for cost reduction is that they are responsible for most of the overall cost. This is due to the numerous air coolers that are required to cool the permeate stream, and the number of DCMD modules to produce the desired amount of water. The cost breakdowns for each module design are shown in Figure 43, Figure 44, and Figure 45. In each case, the primary element of the cost is the air coolers; this shows that despite significant improvements in the modules, the air coolers need improvement in efficiency or another method of cooling must be found.
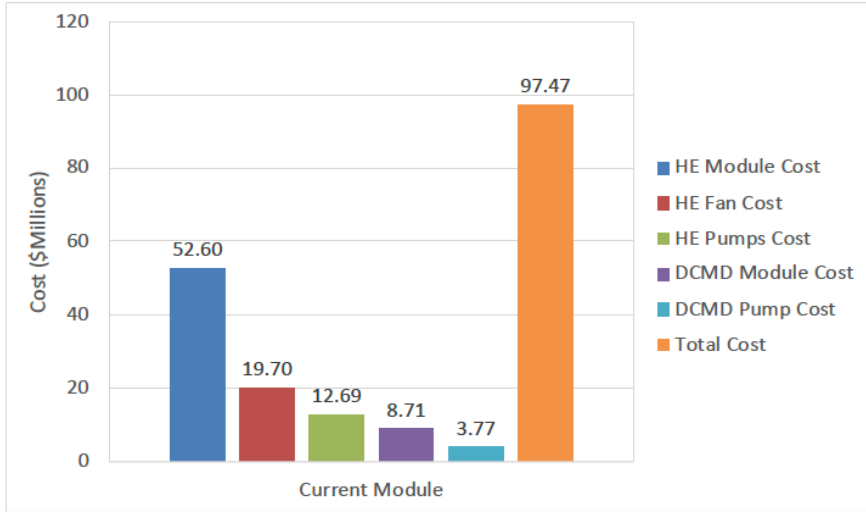
Figure 43. Cost breakdown of the DCMD and HE equipment for the current module design conditions
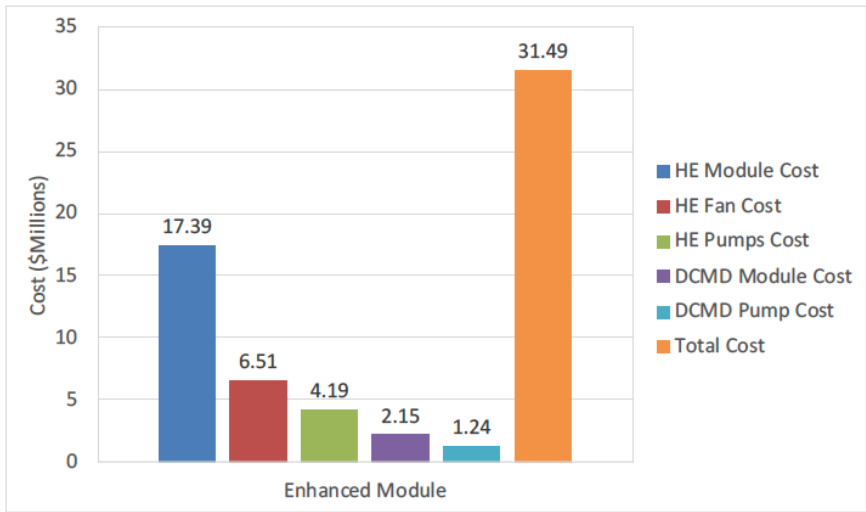

Figure 44. Cost breakdown of the DCMD and HE equipment for the enhanced module design conditions
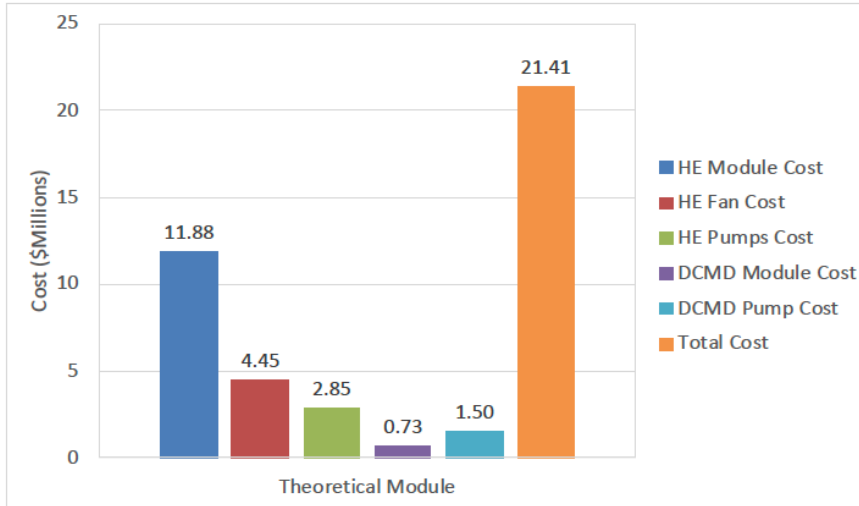
Figure 45. Cost breakdown of the DCMD and HE equipment for the theoretical module design conditions

It can be seen that the increased flow distribution and usable membrane area drive the total cost of the system down significantly. However, the capital costs associated with the system are still enormous. Regardless of the DCMD module design, the limiting factor for these DCMD systems is the air coolers. This is a result of the necessary operating temperatures of DCMD. It can therefore be concluded that improved flow distribution of the module and cooling the permeate stream are the primary constraints for reducing the cost of DCMD systems.

3.3.3. Implications for Large-Scale DCMD Systems

Based on the cost analysis completed for this study, it can be concluded that DCMD is not capable of being applied as a large-scale desalination technology of low salinity aquifers under current or theoretical conditions. This is due to the competitive costs of current RO, multi-effect distillation (MED), and multi-stage flash distillation (MSF) for desalinating water sources having similar concentrations. DCMD modules are severely hindered by their current module design and therefore are limited in application. In order for DCMD to be evaluated as a cost-effective means of enhanced recovery, this issue must be rectified as it permits increased flow rates and fluxes for high water recovery. Air coolers are a significant contributor to the total cost of DCMD as it is difficult to cool such large volumes of permeate water to the desired low temperature. This unit will require increased efficiency in the design if DCMD is to be competitive.

4. Conclusions

The goal of this study was to develop a working model that could accurately predict DCMD module performance – in particular, water flux and water production – given a particular set of

membrane characteristics and operating conditions. In addition, the study sought to develop a techno-economic model that could be used to construct an appraisal level cost estimation of large-scale DCMD systems to determine its viability. A model was successfully constructed in MATLAB to estimate DCMD module performance within a 20 percent tolerance. An Excel add-in was also created to perform model calculations in Excel without the need of MATLAB. Impact studies were conducted to determine the viability of DCMD for industrial applications. The main findings of the study are summarized below.

- DCMD cannot compete with RO as a desalination technology in large-scale water production applications. However, it could be used as a brine concentration technology.
- High permeate flux does not imply higher water production due to the fact that the feed flow rate required to obtain optimal flux performance severely limits the number of modules that could be used in a system.
- System pressure, LEP, and the available volume of geothermal water are limiting factors for improving system performance.
- Membrane thermal conductivity should be reduced to maximize module performance and water production.
- Decreasing wall thickness does not necessarily improve module performance. The high flux at the front of the module causes temperature equilibrium to occur very quickly through latent heat transfer. Consequently, increasing the length of the module does not result in increased water production.
- Permeate inlet temperatures have to be much lower than those that were initially accepted in order to utilize more of the module length.
- Further design research needs to be conducted to improve flow distribution and increase the active surface area within the module.
- Additional experimental data is needed to improve accuracy of shell and lumen pressure models.
- Modules that utilize PVDF and PP hollow fiber should be tested so that the model can be verified for a broader range of module types.
- The cooling of the permeate stream involves an enormous amount of capital cost due to the need of numerous air coolers. Improved air coolers with increased efficiencies may allow for DCMD to be a usable technology.

4.1. Recommended Next Steps

Future research to improve the commercial viability of large-scale DCMD systems for water desalination should focus on the topics identified below.

- Be able to heat the feed and cool the permeate while they are in the modules in order to reduce flow rates and increase flux.
- Increase the recovery efficiency and reuse of low-grade heat so that the overall energy footprint and capital costs of DCMD systems can be reduced.

- Improve module design in order to provide better flow distribution, more effective membrane area, and lower fouling propensity.
- Improve membrane characteristics in LEP in order to provide operational flexibility.

References

El-Bourawi, M.S., Z. Ding, R. Ma, and M. Khayet. 2006. "A Framework for Better Understanding Membrane Distillation Separation Process." *Journal of Membrane Science* 285, pp. 4-29.

Franken, A.C.M., J.A.M. Nolten, M.H.V. Mulder, D. Bargeman, and C.A. Smolders. 1987. "Wetting Criteria for the Applicability of Membrane Distillation." *Journal of Membrane Science*, 33(3), pp. 315–328.

Gleick, P.H. 2010. "Roadmap for Sustainable Water Resources in Southwestern North America." *PNAS* 107, pp. 21300-21305.

Huang, F. Y. C. and A. Arning. 2019. "Performance Comparison between Polyvinylidene Fluoride and Polytetrafluoroethylene Hollow Fiber Membranes for Direct Contact Membrane Distillation." *Membranes*, 9(4), p. 52.

Huang, F.Y.C., L. Laumbach, R. Reprogle, and C. Medin. 2018. "Geothermal Membrane Distillation in Industrial Greenhouse Applications: Membrane Fabrication and Characterization." *Environmental Engineering Science*, 35(8), pp. 815-828.

Huang, F.Y.C., C. Medin, and A. Arning. 2019. "Mechanical Vibration for the Control of Membrane Fouling in Direct Contact Membrane Distillation." *Symmetry* 11(2), p. 126.

Huang, F.Y.C. and R. Reprogle. 2019. "Thermal Conductivity of Polyvinylidene Fluoride Membranes for Direct Contact Membrane Distillation." *Environmental Engineering Science*, 36(4), pp. 420-430.

Lawson, K.W., and D.R. Lloyd. 1997. "Membrane Distillation." *Journal of Membrane Science* 124, pp. 1-25.

Noor, N., J. Koll, N. Scharnagl, C. Abetz, and V. Abetz. 2018. "Hollow Fiber Membranes of Blends of Polyethersulfone and Sulfonated Polymers." *Membranes*, 8(3), p. 54.

Phattaranawik, J., R. Jiraratananon, and A.G. Fane. 2003. "Heat Transport and Membrane Distillation Coefficients in Direct Contact Membrane Distillation." *Journal of Membrane Science*, 212(1-2), pp. 177–193.

Simone, S., A. Figoli, A. Criscuoli, M.C. Carnevale, A. Rosselli, and E. Drioli. 2010. "Preparation of Hollow Fibre Membranes from PVDF/PVP Blends and their Application in VMD." *Journal of Membrane Science* 364, pp. 219-232.

Stanton, J.S., D. Anning, C. Brown, R. Moore, V. McGuire, S Qi, A. Harris, K. Dennehy, P. McMahon, J. Degnan, and J. Bohlke. 2017. *Brackish Groundwater in the United States.* USGS Professional Paper 1833, 185p.

Susanto, H. 2011. "Towards Practical Implementations of Membrane Distillation." *Chemical Engineering and Processing* 50, pp. 139-150.

Tidwell, V.C., B. Moreland, K. Zemlick, B. Roberts, H. Passell, D. Jensen, C. Forsgren, G. Sehlke, M. Cook, and C. King. 2014. Mapping Water Availability, Projected Use and Cost in the Western United States." *Environ. Res. Lett.* 9, 16p.

Tomaszewska, M. 1996. "Preparation and Properties of Flat-Sheet Membranes from Poly(vinylidene fluoride) for Membrane Distillation." *Desalination* 104, pp. 1-11.

Wang, P. and T. Chung. 2015. "Recent Advances in Membrane Distillation Processes: Membrane Development, Configuration Design and Application Exploring." *Journal of Membrane Science* 474, pp. 39-56.

Zhang, J., N. Dow, M. Duke, E. Ostarcevic, J-D Li, and S. Gray. 2010. "Identification of Material and Physical Features of Membrane Distillation Membranes for High Performance Desalination." *Journal of Membrane Science*, 349(1-2), pp. 295–303.
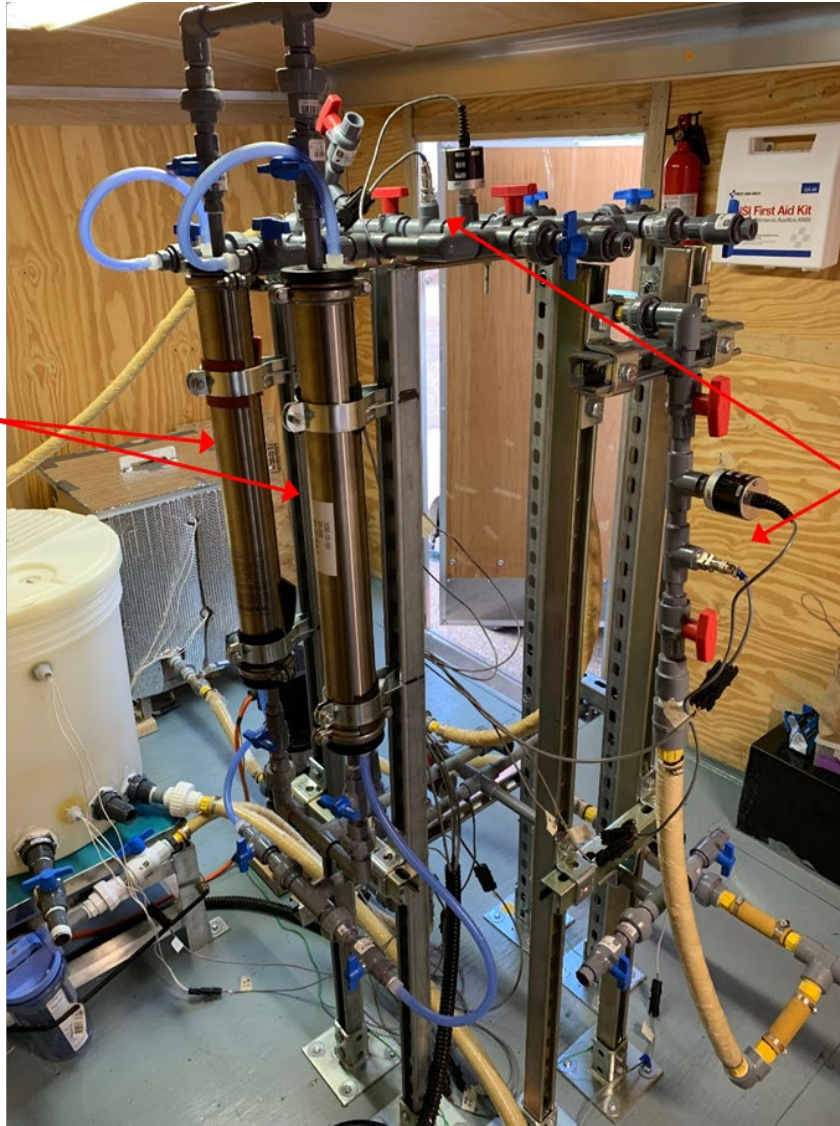
Appendix A

Images of the Completed Pilot-Scale DCMD System
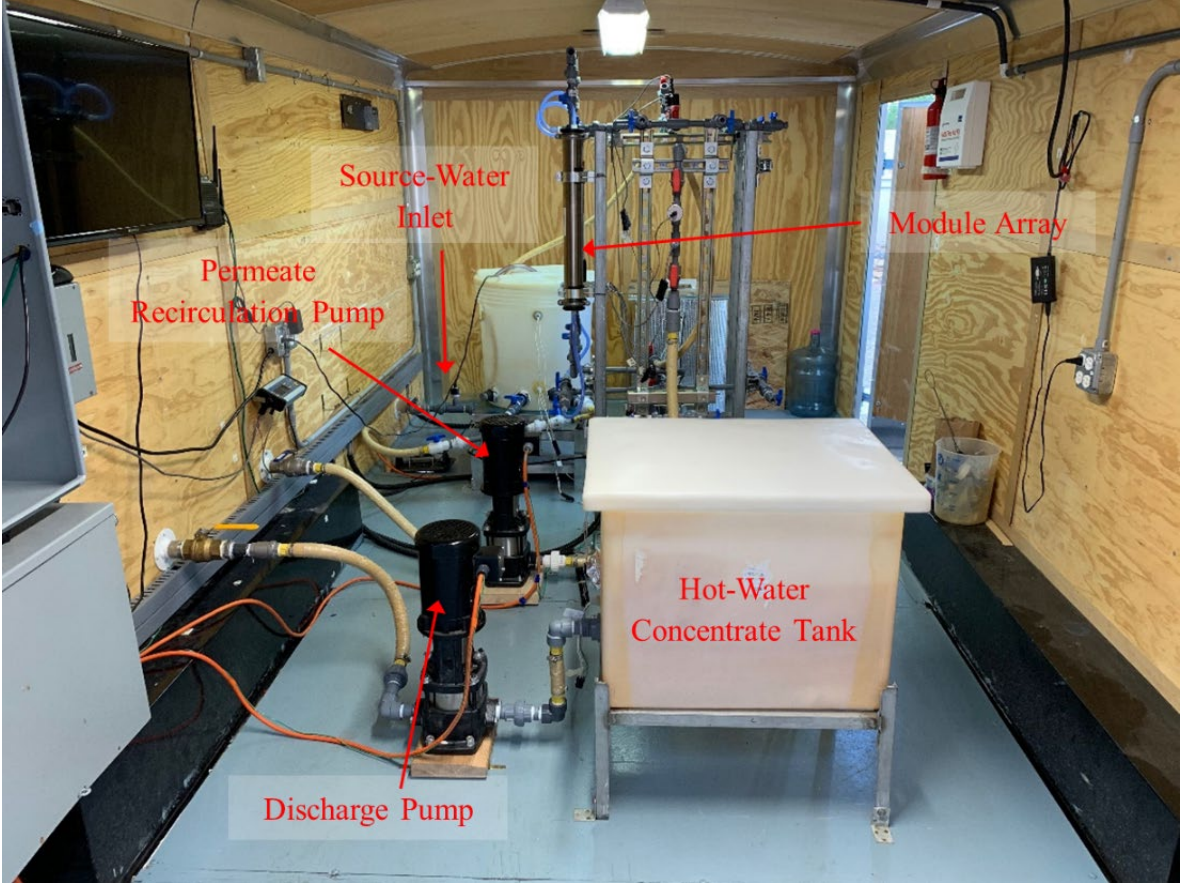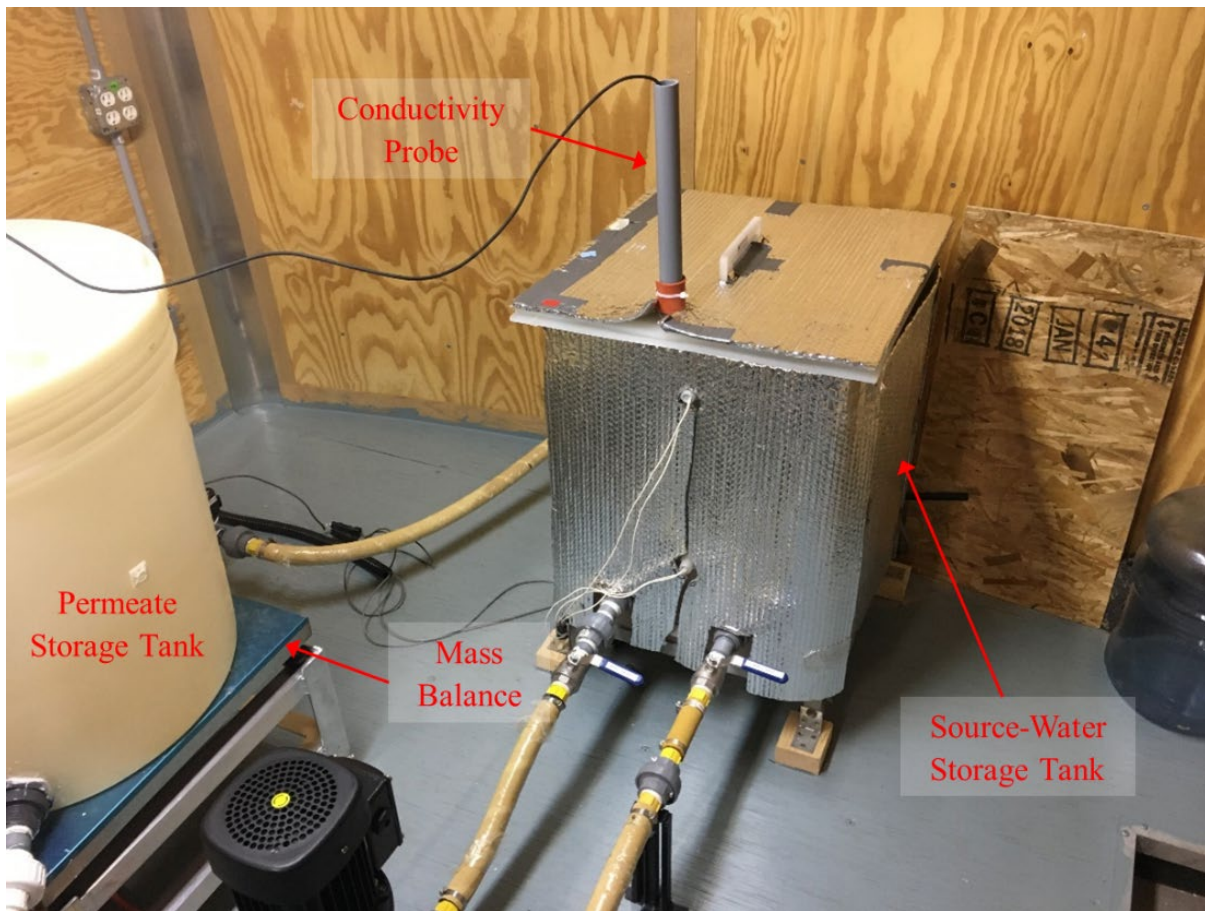
Membrane Module

Sensor Bank

This page intentionally left blank.